enzyme specific for K63 linkage and a partner of RNF8, from HeLa cells by two different siRNAs. The recruitment of GFP-FAAP20 to ICLs was eliminated, as it was in RNF8-depleted cells (Figures 3E and 3F, and Figure S3C), indicating that K63-linked polyubiquitin produced by RNF8-UBC13 is the primary signal for FAAP20 recruitment.

K63-linked ubiquitin chains formed at DSBs are stable and can last at least 4 hr, in contrast to K48-linked chains that are unstable and diminish within 1 hr (Feng and Chen, 2012). The GFP-FAAP20 remained at ICLs for at least 2.5 hr (Figure 3A), consistent with the notion that it recognizes the stable K63-linked chains.

RNF168 Is Largely Dispensable for FAAP20 Recruitment

RNF168 is the second E3 ubiquitin ligase that accumulates at damaged chromatin and amplifies K63-linked polyubiquitination initiated by RNF8-UBC13. Interestingly, the recruitment of GFP-FAAP20 to ICLs was observed in majority of cells depleted of RNF168 by two different siRNAs (83% and 78% for siRNF168-treated cells, compared to 95% for control cells) (Figures 3E and 3F, and Figure S3D). As a control, the recruitment of RNF168 itself to ICLs was eliminated by the same siRNAs (see Figures 5D and 5E). Therefore, RNF168-mediated amplification of the K63 ubiquitin signal is largely dispensable for recruitment of FAAP20.

The Ubiquitin-Binding Activity of FAAP20 Is Required for Normal Recruitment of the FA Core Complex and FANCD2 to ICLs

We studied whether the RNF8-FAAP20 cascade controls recruitment of the FA core complex and FANCD2 to ICLs. We observed recruitment of both FANCA and FANCD2 to ICLs (Figure 4A). The data are in agreement with earlier findings that FA proteins function at ICLs (Ben-Yehoyada et al., 2009; Knipscheer et al., 2009; Shen et al., 2009; Yan et al., 2010). Importantly, the recruitment of both FANCA and FANCD2 was strongly diminished in cells depleted of FAAP20 (Figures 4A and 4B), indicating that FAAP20 is required for normal recruitment of the FA core and ID complexes to ICLs. Notably, introduction of an siRNA-resistant version of FAAP20 into FAAP20 siRNA-treated cells partially rescued the recruitment of FA core complex and FANCD2, whereas the FAAP20-D164A mutant failed to rescue (Figures 4C–4E; and Figure S4A). In fact, even when cells were treated with control siRNA, those expressing FAAP20-D164A mutant had 90% reduction of FANCA and 40% reduction of FANCD2 recruitment compared those expressing wild-type FAAP20, indicating that the UBZ mutant acts dominant-negatively to inhibit the recruitment process. The data suggest that the ubiquitin-binding activity of FAAP20 is needed for recruitment not only of itself (Figures 3B–3D) but also of the FA core complex and FANCD2.

The Ubiquitin-Binding Activity of FAAP20 Is Required for Normal Activation of the FA Pathway

We investigated whether the ubiquitin-binding activity of FAAP20 is needed for FA pathway activation using *FAAP20*$^{-/-}$ DT40 cells. The *FAAP20*$^{-/-}$ cells had a lower level of monoubiquitinated FANCD2 (Figure 4F and Figure S4B) as well as a reduced number of FANCD2 nuclear foci in response to MMC treatment (Figures 4G and 4H); introduction of wild-type FAAP20 largely corrected both defects. In contrast, introduction of FAAP20 carrying either C147A or D164A substitutions failed to correct these defects (Figures 4F–4H, and Figures S4C and S4D). Because both mutants lack ubiquitin-binding activity, the data suggest that this activity of FAAP20 is required for optimal activation of the FA pathway.

A FAAP20 mutant that lacked the UBZ domain coimmunoprecipitated normally with FANCA (Figures S4E and S4F), suggesting that the failure of the UBZ domain mutants to restore the FA pathway is not due to their inability to assemble into the FA core complex. Another FAAP20 mutant lacking the N-terminal 65 residues failed to coimmunoprecipitate with FANCA (Figures S4E and S4F), indicating that this region is required for FAAP20 assembly into the core complex.

RNF8 and Its Ubiquitinated Product Accumulate at ICLs Earlier Than FA Proteins

RNF8 accumulates rapidly at DSBs to promote K63-linked ubiquitination on H2A-type histones (Huen et al., 2007; Kolas et al., 2007; Marteijn et al., 2009; Wang and Elledge, 2007). We found that RNF8 and its product, ubiquitinated H2A, accumulated at laser-activated ICLs within minutes after photoactivation (Figures 5A and 5B). The appearance of RNF8 preceded that of ubiquitinated H2A (approximately 1 min versus 3 min) (Figure 5A), consistent with a sequential process in which RNF8 is first recruited by an upstream signal and then ubiquitinates H2A at the site of damage.

The accumulation of RNF8 and ubiquitinated H2A at ICLs precedes that of FANCA and FANCD2 (1 and 3 min versus 5 and 10 min) (Figure 5A), suggesting that RNF8-initiated ubiquitination signals (ubiquitinated H2A or other substrates) act earlier in a cascade to recruit FANC proteins to ICLs.

The Recruitment of FANCA and FANCD2 to ICLs Requires RNF8

The data above suggested a hierarchy in control of FA proteins: RNF8 is required for recruitment of FAAP20, which is in turn needed for recruitment of FA core complex and FANCD2.

(B and C) Images (B) and a graph (C) show that GFP-FAAP20 wild-type (WT) was recruited to ICL sites, but the GFP-FAAP20-D164A mutant was not. Immunostaining of γ-H2AX marks the areas targeted by the laser and also serves as a control to show a positive DNA damage response. Error bars in (C) are standard deviations.

(D) (Top panel) Schematic representation of the plasmid substrates used in the eChIP assay. The presence of psoralen-ICL is indicated. (Bottom panel) A graph from eChIP shows that FAAP20 wild-type (WT) protein was enriched about 4-fold at the ICL, whereas FAAP20-D164A mutant was not. Error bars represent standard deviations from three independent experiments.

(E and F) Images (E) and graphs (F) show the recruitment of GFP-FAAP20 to ICLs in HeLa cells transfected with two different siRNAs against RNF168, RNF8, or UBC13, respectively. Error bars in (F) are standard deviations (see also Figure S3).

Please cite this article in press as: Yan et al., A Ubiquitin-Binding Protein, FAAP20, Links RNF8-Mediated Ubiquitination to the Fanconi Anemia DNA Repair Network, Molecular Cell (2012), doi:10.1016/j.molcel.2012.05.026

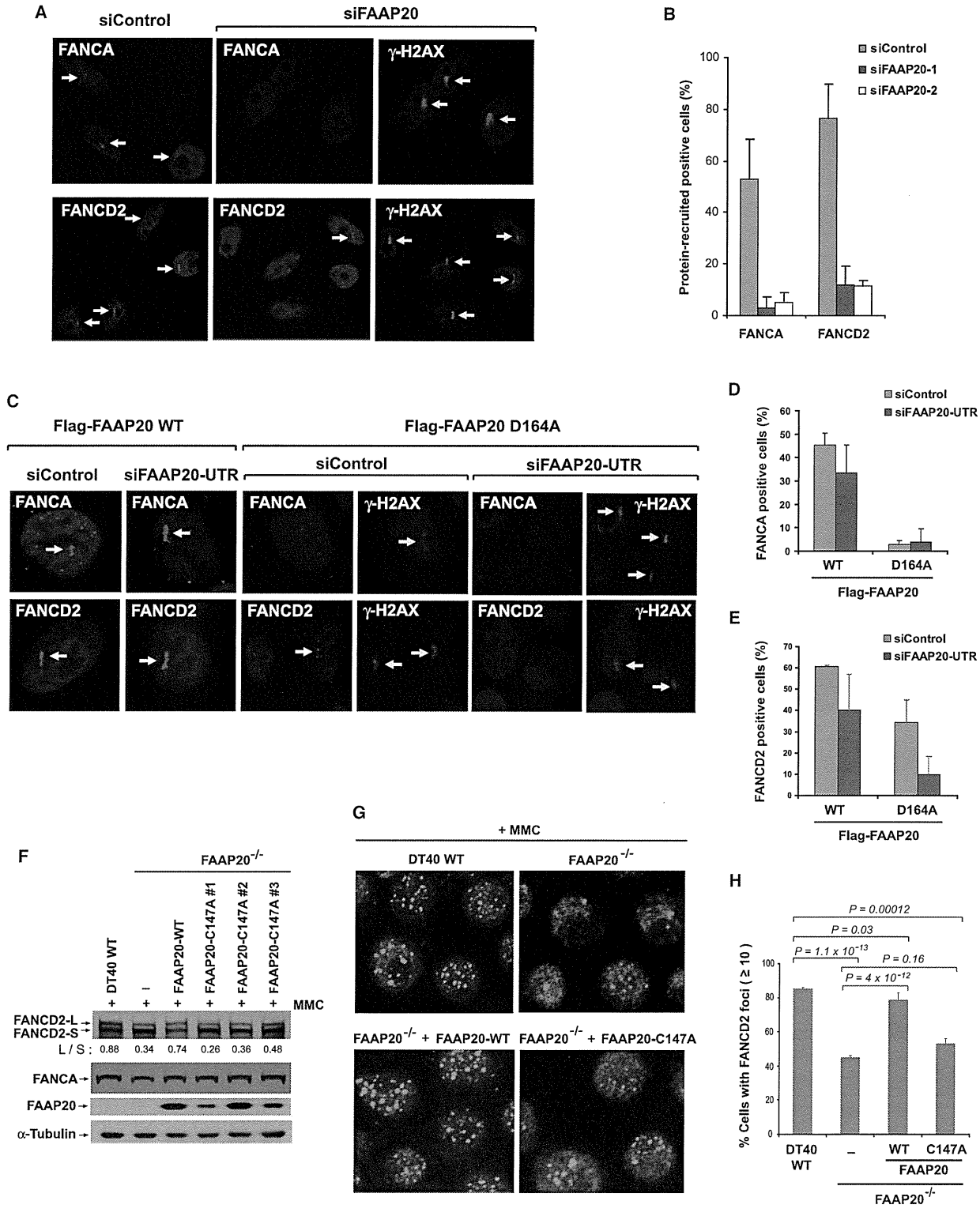

The data predict that RNF8 should also be required for recruitment of FA core complex and FANCD2. In agreement with this notion, depletion of RNF8 by two different siRNAs in HeLa cells not only disrupted induction of ubiquitinated H2A but also substantially reduced the accumulation of FANCA and FANCD2 at ICLs (Figures 5B and 5C). These data suggest that RNF8 acts upstream of FA core complex and FANCD2 to promote their recruitment to ICLs.

RNF168 Affects Efficiency of the Recruitment of FANC Proteins to ICLs

Like RNF8, RNF168 also accumulated at ICLs, and its appearance was after RNF8 but before FANCA and FANCD2 (Figures 5A and 5D). However, depletion of RNF168 by two different siRNAs had only a modest effect on recruitment of FANCA and FANCD2: about 50% reduction for the former and 20% for the latter (Figure 5E). This is in contrast to the depletion of RNF8, which reduced recruitment of FANCA and FANCD2 by about 90% and 80%, respectively. These data are reminiscent of the findings that RNF168 depletion does not significantly affect recruitment of GFP-FAAP20 (Figures 3E and 3F). Thus, while RNF8 plays a critical role for recruitment of FANC proteins to ICLs, RNF168 only affects the efficiency of the recruitment.

RNF8 Is Dispensable for Recruitment of FANCM to ICLs

We have previously shown that most FANCM and its DNA binding partner MHF (about 90%) do not associate with the FA core complex but are present in the distinct FANCM-MHF complex that lacks FANCA and other FANC proteins. Moreover, the recruitment of FANCM-MHF to laser-activated psoralen ICLs only occurs in S phase cells (Yan et al., 2010). This is in contrast to recruitment of RNF8, GFP-FAAP20, FANCA, and FANCD2 that occurred in most (80% or more) unsynchronized HeLa cells (Figure 3C and Figure 5A; less than 20% of these cells are in S phase [data not shown]). The data imply that recruitment of FANCM-MHF in the S phase is different from the RNF8-dependent recruitment of FANCA and FANCD2, which can occur independently of cell-cycle phase. In support of this notion, the recruitment of FANCM was unaffected in RNF8-depleted cells (Figures 5B and 5C), in contrast to recruitment of FANCA and FANCD2, which was disrupted. Together, the data suggest that RNF8-mediated ubiquitination is dispensable for FANCM recruitment during S phase.

RNF8 Promotes Efficient Activation of the FA Network and Works in the Same Pathway as the FA Core Complex in Cellular Resistance to ICLs

Our findings that RNF8 is required for recruitment of FANC proteins to ICLs prompted us to study if it is also needed for activation of the FA network. We found that HeLa cells depleted of RNF8 by two different siRNAs exhibited a reduced level of monoubiquitinated FANCD2 (Figure 6A) and a decreased number of FANCD2 nuclear foci in response to MMC (Figures 6B and 6C). The reduced FANCD2 monoubiquitination was not due to inability of the depleted cells to enter S phase, because the percentage of S phase cells in RNF8-depleted cells was comparable to that of control cells (Figure S5A). Moreover, RNF8-depleted cells displayed increased sensitivity to MMC (Figures S5B and S5C). These features resemble those of cells deficient in FA core complex and suggest that RNF8 is required for normal function of the FA pathway.

Importantly, cells doubly depleted of both RNF8 and FANCA exhibited MMC sensitivity similar to that of single gene-depleted cells (Figures 6D and 6E), suggesting that RNF8 and FA core complex act in the same pathway to resist MMC-induced DNA damage.

The RNF8-FAAP20 Cascade Is Required for Recruitment of FA Core Complex and FANCD2 to DSBs

The FA network can be activated not only by ICLs but also by other DNA damage, including DSBs (Garcia-Higuera et al., 2001). We asked if FANC proteins are recruited to DSBs, and if they do, whether their recruitment also depends on the RNF8-FAAP20 cascade. We found that both FANCA and FANCD2 were recruited to laser-activated DSBs (Figures S6A and S6B). Importantly, recruitment of both FANC proteins was strongly abrogated in cells depleted of either FAAP20 (Figures S6A and S6B) or RNF8 (Figures S6C and S6D). The data suggest that the RNF-FAAP20 cascade may be part of a general pathway that governs recruitment of FANC proteins to multiple forms of DNA damage.

DISCUSSION

RNF8 and FAAP20 Constitute a Ubiquitin Signaling Cascade

Phosphorylation of several subunits of the FA core complex by ATR and its downstream kinase CHK1 has been shown to regulate monoubiquitination of FANCD2, a key function of the

Figure 4. The Ubiquitin-Binding Activity of FAAP20 Is Required for Recruitment of FA Core Complex and FANCD2 and for Normal Activation of the FA Pathway

(A and B) Images (A) and a graph (B) show that HeLa cells depleted of FAAP20 by two siRNAs are deficient in the recruitment of FANCA and FANCD2 to ICL sites. Immunostaining of γ-H2AX indicates the areas targeted by the laser and also serves as a control to show a positive DNA damage response. The positive recruitment signals are indicated by arrows. Error bars in (B) are standard deviations.

(C–E) Images (C) and graphs (D and E) show the recruitment of FANCA and FANCD2 at ICLs in HeLa cells stably expressing an siRNA-resistant version of Flag-FAAP20 wild-type (WT) or D164A mutant. These cells were treated with either a nontargeting siRNA (siControl) or a siRNA targeting the 3′ untranslated region of human FAAP20 (siFAAP20-UTR). Error bars in (D) and (E) are standard deviations.

(F) Immunoblotting shows the levels of monoubiquitinated (L) and nonubiquitinated (S) FANCD2 in lysates from various DT40 cells (wild-type [WT], *FAAP20*$^{-/-}$ cells, and *FAAP20*$^{-/-}$ cells complemented with human FAAP20 wild-type [WT] and C147A mutant version [three independent clones]). Cells were treated with 500 ng/ml MMC for 6 hr.

(G and H) Immunostaining images (G) and a graph (H) show FANCD2 nuclear foci in various DT40 cells treated with MMC. The error bars in (H) are standard deviations. p values between different cell lines are shown (see also Figure S4).

Please cite this article in press as: Yan et al., A Ubiquitin-Binding Protein, FAAP20, Links RNF8-Mediated Ubiquitination to the Fanconi Anemia DNA Repair Network, Molecular Cell (2012), doi:10.1016/j.molcel.2012.05.026

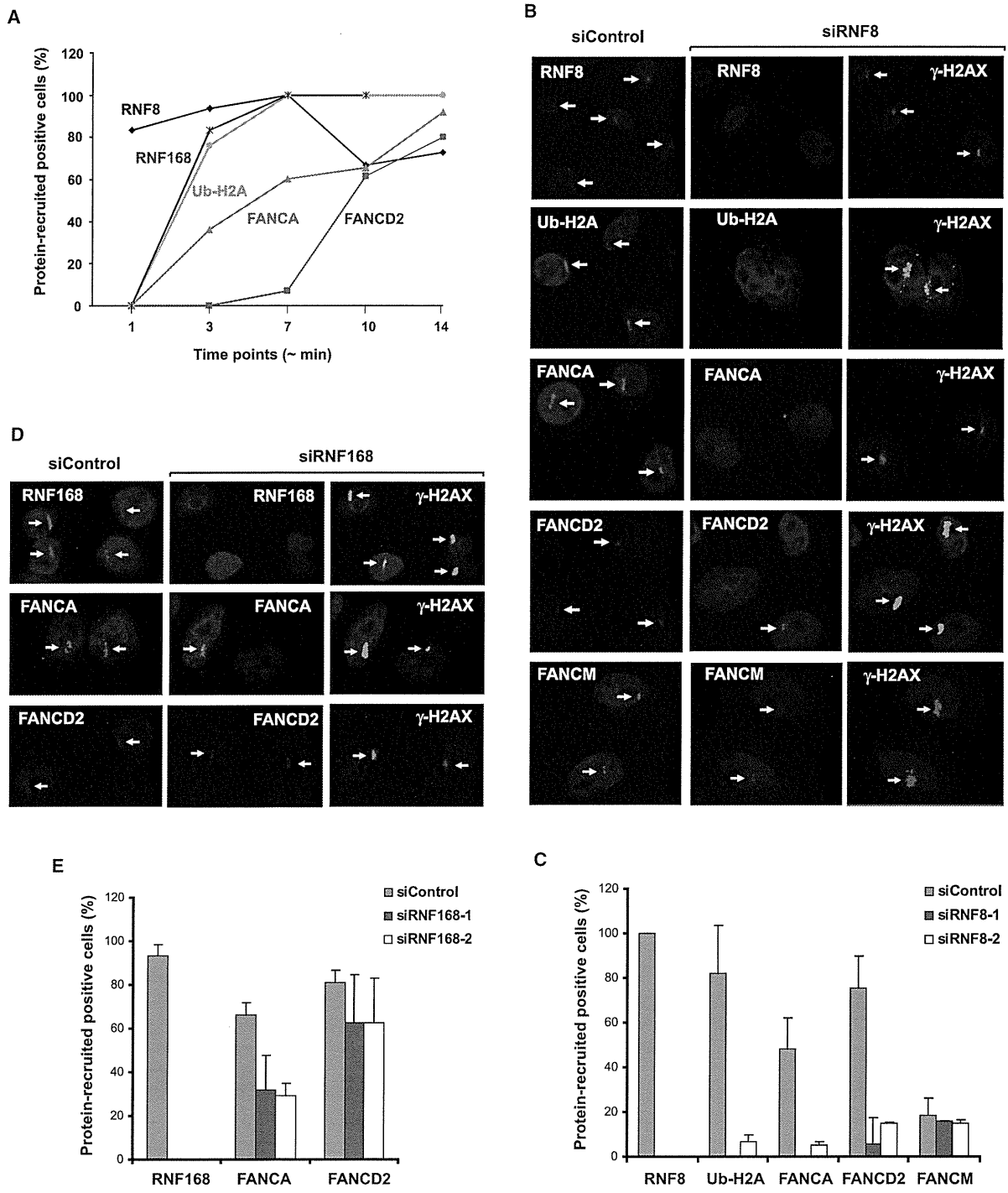

Figure 5. RNF8 Is Required for Recruitment of FANCA and FANCD2 to ICLs, but Not for FANCM Recruitment

(A) A time course study shows the sequential recruitment of RNF8, RNF168, Ub-H2A, FANCA, and FANCD2 to psoralen-induced ICLs after laser activation.

(B and C) Images (B) and a graph (C) show that HeLa cells depleted of RNF8 by two siRNAs are deficient in accumulation of ubiquitinated H2A (Ub-H2A), FANCA, and FANCD2 at ICLs; but they are normal in accumulation of FANCM. Immunostaining of γ-H2AX marks the areas targeted by the laser and also serves as a control to show a positive DNA damage response. The recruitment signals are indicated by arrows. Error bars are standard deviations.

(D and E) The same as described in (B) and (C), except siRNAs targeting RNF168 are used.

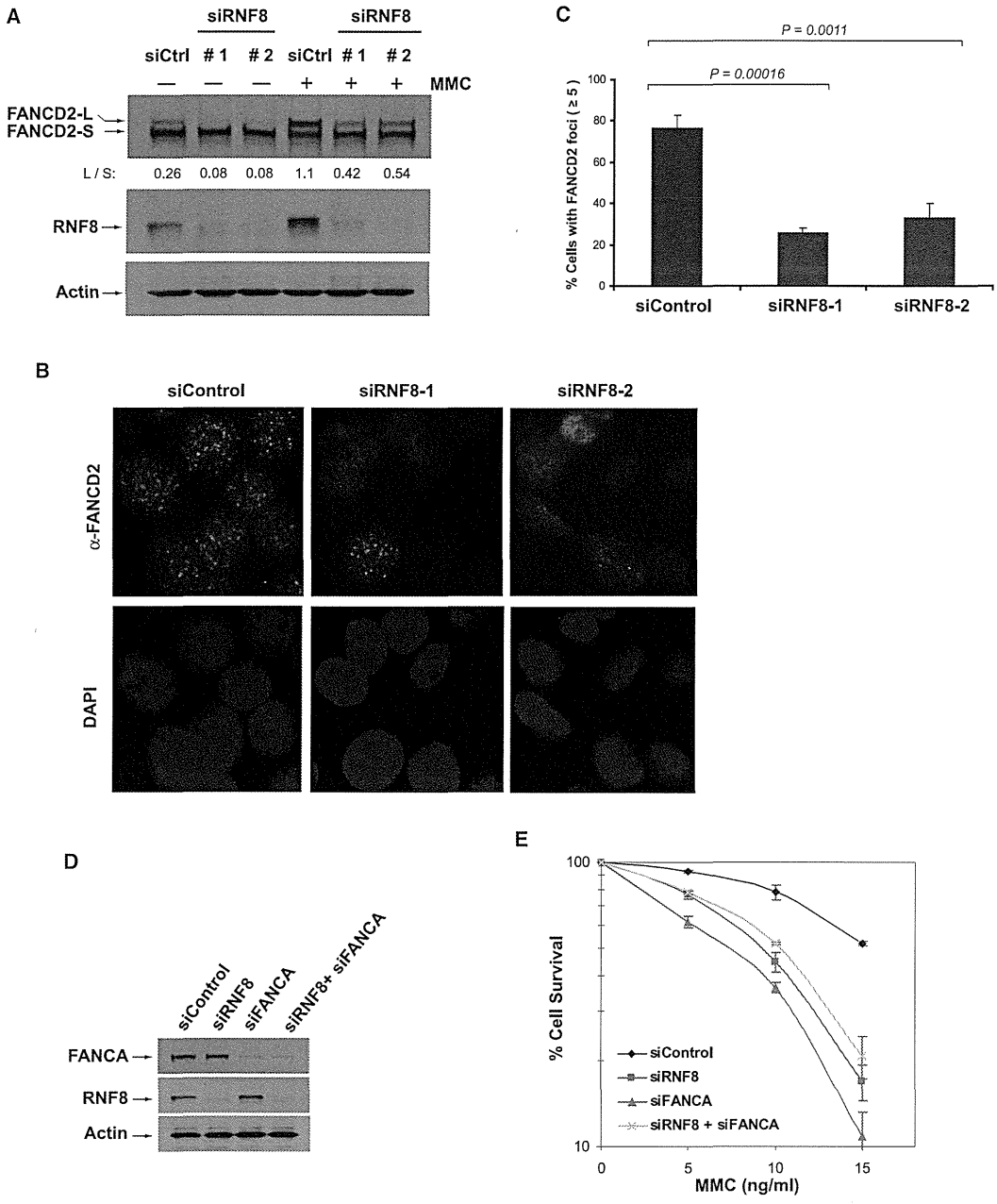

Figure 6. RNF8 Is Required for Efficient FANCD2 Monoubiquitination and Focus Formation and Works in the Same Pathway as the FA Core Complex in Cellular Resistance to ICLs

(A) Immunoblotting shows that HeLa cells depleted of RNF8 by two different siRNAs have a reduced level of monoubiquitinated FANCD2 in the absence or presence of MMC (60 ng/ml for 16 hr).

(B and C) Immunostaining (B) and a graph (C) show that HeLa cells depleted of RNF8 by two siRNAs have a decreased number of FANCD2 nuclear foci in the presence of MMC. Error bars are standard deviations. p values are shown in the top.

(D) Immunoblotting shows the levels of FANCA and RNF8 in lysates from HeLa cells treated with various siRNAs as indicated.

(E) Clonogenic survival assays of HeLa cells depleted of RNF8 or FANCA or doubly depleted of both by siRNAs following the treatment with MMC. The mean surviving percentages with standard error of the mean (SEM) from three independent experiments are shown (see also Figure S5).

Please cite this article in press as: Yan et al., A Ubiquitin-Binding Protein, FAAP20, Links RNF8-Mediated Ubiquitination to the Fanconi Anemia DNA Repair Network, Molecular Cell (2012), doi:10.1016/j.molcel.2012.05.026

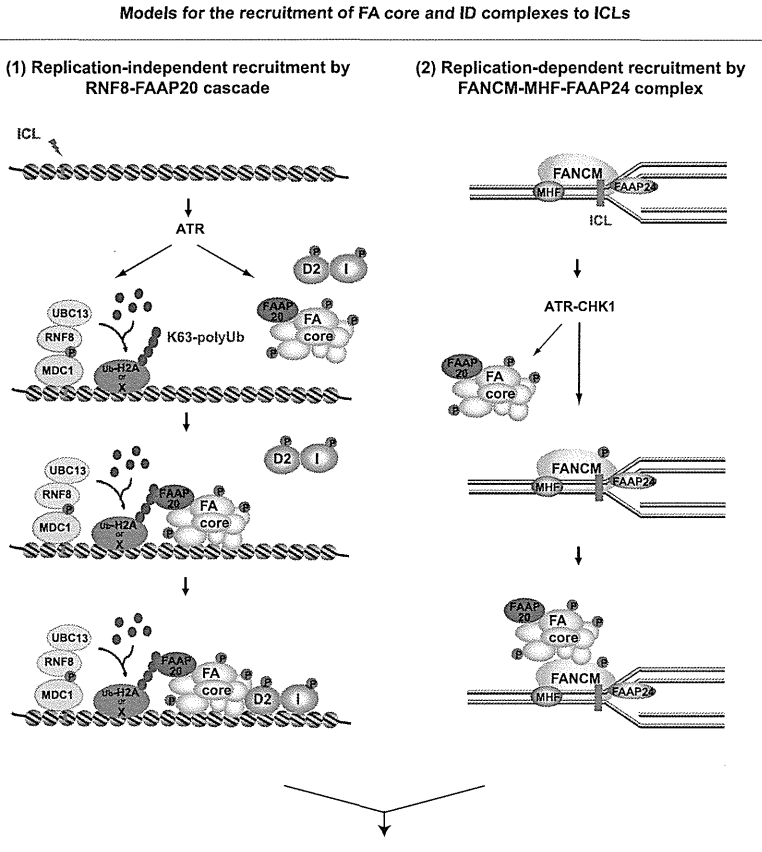

Figure 7. Models for the Recruitment of FA Core Complex and FANCD2 to ICLs by Two Different Pathways

The first pathway is replication independent and controlled by the RNF8-FAAP20 cascade. In keeping with the literature on the activation of the DNA damage response by DSBs, ICLs may activate ATR, which can phosphorylate MDC1 and FANC proteins. RNF8 and UBC13 are recruited to initiate K63-linked polyubiquitination of histone H2A and other substrates (marked by "X") in surrounding chromatin, which are recognized by the UBZ domain of FAAP20 to trigger the recruitment of FA core complex. The FA ID complex is possibly recruited by interacting with the FA core complex. The second pathway is replication dependent and governed by FANCM-MHF-FAAP24 complex. In S phase, FANCM-MHF-FAAP24 complex recognizes ICL-stalled replication forks, activates ATR and CHK1 (Collis et al., 2008), and recruits the FA core complex by direct protein-protein interactions. Both pathways lead to FANCD2 monoubiquitination, the key step of the FA network (see also Figure S6).

core complex (Collins et al., 2009; Wang et al., 2007) (Figure 7). Here we show that the core complex is also governed by a ubiquitin signaling cascade, which is initiated by RNF8 and its partner UBC13, and mediated by FAAP20, a component of the FA core complex. RNF8 and UBC13 act upstream of this cascade, because depletion of either protein abolished the recruitment of GFP-FAAP20 to ICLs. Conversely, FAAP20 functions downstream, as FAAP20 can bind K63-linked polyubiquitin, the product of RNF8-UBC13, in vitro; and the FAAP20 mutant defective in this ubiquitin-binding activity failed to accumulate at ICLs in vivo. Consistent with the proposed role of RNF8 in regulating FA network, our epistasis analyses showed that RNF8 and FANCA work in the same pathway to resist MMC-induced cell killing.

The RNF8-FAAP20 Cascade Is Essential for Recruitment of FA Core Complex to ICLs and for Efficient Activation of the FA Pathway

Our time course analyses revealed a sequential accumulation process of repair proteins at ICLs (Figure 5A). This sequential process suggests a model of how RNF8 regulates the recruitment of FANC proteins (Figure 7). In response to ICLs, RNF8 is recruited to the damage site, where it works with UBC13 to catalyze K63-linked ubiquitination of histone H2A and possibly other substrates in chromatin flanking the lesions. The ubiquitinated H2A (and perhaps other ubiquitinated molecules) then interacts with the UBZ domain of FAAP20 to recruit the FA core complex to damaged chromatin. Finally, FANCD2 is recruited, possibly by interacting with the FA core complex already bound at the ICLs. This model is supported by the siRNA data showing that RNF8 depletion disrupted accumulation of all downstream proteins at ICLs, and that FAAP20 depletion reduced FANCA and FANCD2 recruitment. It is also supported by the evidence that the ubiquitin-binding activity of FAAP20 is needed for recruitment of FANCA and FANCD2.

The RNF8-FAAP20 cascade also plays a regulatory albeit nonessential role in modulating the efficiency of FANCD2 monoubiquitination, a key step of the FA network. This is evidenced by observations that HeLa cells depleted of either RNF8 or FAAP20, and DT40 cells inactivated of FAAP20, all displayed reduced levels of MMC-induced FANCD2 monoubiqutination and redistribution to nuclear foci.

FANCM Is Recruited to ICLs through a Pathway Independent of RNF8

Why is the RNF8-FAAP20 cascade essential for recruitment of FA core complex to psoralen-activated ICLs but nonessential for MMC-induced FANCD2 monoubiquition? One explanation is that there exists another pathway independent of the RNF8-FAAP20 cascade that can also promote FANCD2 monoubiquitination (Figure 7). It should be pointed out that ICLs generated by psoralen and MMC are structurally different so that they may be detected by distinct mechanisms, leading to different responses (Muniandy et al., 2010). The psoralen ICLs distort DNA duplex

so that they can be rapidly detected by DNA damage sensors in any phase of the cell cycle to activate the RNF8-FAAP20 cascade. In contrast, MMC ICLs do not significantly distort DNA duplex, so they may remain largely undetected until S phase, when they block progression of replication forks. The blocked forks may be recognized by FANCM-MHF (and possibly FAAP24), which recruits the FA core complex through direct protein-protein interactions. In agreement with this notion, the recruitment of FANCM-MHF to ICLs of psoralen occurred only during S phase (Yan et al., 2010) and was unaffected when RNF8 was depleted (Figures 5B and 5C). Thus, at least two pathways regulate the FA core complex recruitment: one is replication independent, and the other one is replication dependent. Only the first one depends on the RNF8-FAAP20 cascade, whereas the latter one depends on FANCM and its DNA-binding partners. Cells deficient in either pathway are partially defective in FANCD2 monoubiquitination. We predict that only when both pathways are disrupted will FANCD2 monoubiquitination be eliminated.

K63-Linked Polyubiquitin Generated by RNF8-UBC13 Signals FAAP20 Recruitment

RNF8 can promote ubiquitination of both K63- and K48-linked chains at DSBs (Feng and Chen, 2012; Lok et al., 2011). We found that the UBZ domain of FAAP20 can bind both chains but has a preference for K63 linkage. Our findings that cells depleted of UBC13, the E2 enzyme specific for K63-linked polyubiquitination, are completely deficient in recruiting GFP-FAAP20 to ICLs indicate that the K63 linkage is the primary signal. In support of this notion, inhibition of K63-linked polyubiquitination sensitizes cells to agents that induce ICLs (Chiu et al., 2006); and cells deficient in UBC13 are sensitive to ICL-inducing drugs (Zhao et al., 2007). The observation that K48 chains are bound by FAAP20 in vitro, but do not appear to be effective binding partners in vivo (because UBC13 depletion eliminated FAAP20 recruitment even though K48 chains would be present), suggests that recognition of K48 by FAAP20 may be suppressed in vivo, perhaps outcompeted by proteins with higher affinity for K48.

RNF168 Affects Efficiency of the Recruitment of FA Proteins to ICLs

RNF8 and RNF168 ubiquitin ligases work coordinately to catalyze K63-linked polyubiquitination at chromatin regions surrounding DSBs or UV-induced damage sites, and both are required for recruitment of several downstream repair molecules. Our data suggest that the RNF8-initiated K63-linked polyubiquitination signal is sufficient for recognition by the UBZ domain of FAAP20, leading to recruitment of FA core complex and FANCD2; further amplification of the signal by RNF168 is not necessary but can increase the amount of the recruited FANC proteins. Notably, this selective dependence on RNF8 over RNF168 has been observed for accumulation of RAD51 recombinase at ssDNA lesions in response to replication stress induced by hydroxyurea (Sy et al., 2011). Perhaps cells may have developed different ubiquitin-binding domains (UBDs) to distinguish different K63-linked polyubiquitin signals produced by RNF8 and RNF168. The FAAP20-UBZ domain may represent one type of UBDs that can bind shorter K63-linked chains generated by RNF8, whereas the UBDs in some other proteins may only recognize elongated K63 chains produced by RNF168.

The Ubiquitin-Binding Activity of FAAP20 Is Essential for Recruitment of FA Core Complex to ICLs and for Optimal Activation of the FA Pathway

While our manuscript was under revision, three groups independently reported that FAAP20 is part of the FA core complex and required for optimal activation of the FA pathway (Ali et al., 2012; Kim et al., 2012; Leung et al., 2012), consistent with our findings. However, the conclusions regarding the ubiquitin-binding activity of FAAP20 are controversial. First, Ali et al. showed that FAAP20 does not bind monoubiquitin, in agreement with our data, whereas Kim et al. proposed that FAAP20 binds Rev1, and this binding is enhanced by monoubiquitination of Rev1. However, examination of the data from Kim et al. suggests that FAAP20 appears to bind better to nonubiquitinated than monoubiquitinated Rev1 (the ratio between the nonubiquitinated and monoubiquitinated form was increased in their FAAP20 immunoprecipitate compared to the pre-IP extract, their Figure 4C, lane 7 versus lane 3); and FAAP20 with mutated UBZ domain can still bind Rev1 (their Figure 4C, lane 8). One interpretation, which fits data from all groups, is that FAAP20 may bind nonubiquitinated Rev1 through a ubiquitin-independent mechanism, and this binding may be decreased by monoubiquitination. Second, Ali et al., using FAAP20-depleted HeLa cells, concluded that the ubiquitin-binding activity of FAAP20 is necessary for normal activation of the FA pathway, whereas Leung et al., using FAAP20-inactivated HCT116 cells, concluded that it is dispensable. Our data from FAAP20-knockout DT40 cells and FAAP20-depleted HeLa cells suggest that this activity is not only important for normal activation of the FA pathway but also critical for recruitment of the FA core complex to ICLs. The lack of importance for this activity in HCT116 cells might be because this cell line carries mutations in MRE11 and MLH1, which are involved in activation of ATR (Nam and Cortez, 2011), resulting in aberrant response to replication stress (Wen et al., 2008). We found that recruitment of FA proteins to ICLs in HCT116 cells is about 50% lower compared to that in HeLa cells (data not shown), suggesting that the RNF8-FAAP20 cascade may be inefficiently utilized and thus less important in this cell line.

In summary, our data suggest that the FA core complex is governed not only by phosphorylation but also by the RNF8-FAAP20 ubiquitin cascade. Our data showing that the recruitment of the FA core complex and FANCD2 to DSBs also depends on RNF8 and FAAP20 suggest that this cascade can respond to many forms of DNA damage.

EXPERIMENTAL PROCEDURES

Cell Lines

Human HeLa and HEK293 cells were grown in DMEM medium supplemented with 10% fetal bovine serum (FBS). Chicken DT40 cells were grown in RPMI-1640 medium supplemented with 10% fetal calf serum, 1% chicken serum, 10 mM HEPES, and 1% penicillin-streptomycin mixture in a 5% CO_2 incubator at 39.5°C. HeLa cells stably expressing Flag-FAAP20 WT and D164A mutant used in eChIP assay were kindly provided by Dr. A.R. Meetei (Ali et al., 2012).

Please cite this article in press as: Yan et al., A Ubiquitin-Binding Protein, FAAP20, Links RNF8-Mediated Ubiquitination to the Fanconi Anemia DNA Repair Network, Molecular Cell (2012), doi:10.1016/j.molcel.2012.05.026

Antibodies

An anti-human FAAP20 antibody was raised against a chimeric protein containing a region of human FAAP20 (aa 67–180) fused to maltose-binding protein (New England Biolabs). An anti-chicken FANCA antibody was raised against a chimeric protein containing a region of chicken FANCA (aa 1698–1944) fused to maltose-binding protein. Anti-chicken FANCD2 and FANCI antibodies were generated in rabbits by injection of recombinant whole-chicken FANCD2 protein (Yamamoto et al., 2011) and partial chicken FANCI protein (aa 1–125), respectively. An anti-RNF168 antibody was kindly provided by Dr. D. Durocher. Anti-RNF8 and anti-UBC13 antibodies were purchased from Abcam. An anti-ubiquitinated histone H2A antibody was purchased from Millipore. An anti-ubiquitin antibody was purchased from Cell Signaling. Other antibodies have been previously described (Yan et al., 2010).

Protein Recruitment to Laser-Induced Localized ICLs

We followed a previous protocol to detect proteins recruited at laser-induced localized ICLs (Muniandy et al., 2009). Briefly, cells were seeded in a 35 mm glass bottom culture dish (MatTek) and were incubated with 6 μM trioxalen at 37°C for 20 min prior to laser treatment. Localized irradiation was performed using the Nikon Eclipse TE2000 confocal microscope equipped with an SRS NL100 nitrogen laser-pumped dye laser (Photonics Instruments, St Charles, IL) that fires 5 ns pulses with a repetition rate of 10 Hz at 365 nm, with a power of 0.7 nW, measured at the back aperture of the 60× objective. The laser was directed to a specified rectangular region of interest (ROI) within the nucleus of a cell visualized with a Plan Fluor 60×/NA 1.25 oil objective. The laser beam was oriented by galvanometer-driven beam displacers and fired randomly throughout the ROI until the entire region was exposed. Throughout an experiment, cells were maintained at 37°C, 5% CO_2, and 80% humidity using an environmental chamber. Cells were fixed immediately in freshly prepared 4% formaldehyde in PBS for 10 min at room temperature, followed by immunostaining.

Detecting Proteins Recruited to a Site-Specific Psoralen-ICL by eChIP

The eChIP was carried out as described (Shen et al., 2009). Percentages of relative enrichment of FAAP20 at the ICL site were arrived by normalizing comparative concentration (from real-time PCR) of each sample with that of its input.

siRNA Experiments

HeLa cells were transfected with siRNA oligos using Lipofectamine RNAi MAX (Invitrogen) according to the manufacturer's protocol. The siRNA oligos used are listed in the Supplemental Information.

Expression and Purification of GST-Fusion Proteins from *E. coli*

The expression plasmid for GST-FAAP20-UBZ domain (pGEX-FAAP20-UBZ) was constructed by cloning a region of human FAAP20 that includes the UBZ domain into the BamHI and EcoRI sites of pGEX-2TK. *E. coli* Rosetta (Novagen) cells carrying pGEX-UBZ-wild-type construct or its mutant versions were grown at 30°C to OD_{600} of 0.4–0.5, and 200 μM $ZnCl_2$ (final concentration) was added to culture. When OD_{600} reached 0.6–0.8, cells were induced with 0.2 mM IPTG at 30°C for 3 hr. Cell pellets were resuspended in lysis buffer (25 mM sodium phosphate [pH 8.0], 300 mM NaCl, 10% glycerol) containing lysozyme, DNase I, benzonase, and complete EDTA-free protease inhibitor cocktail (Roche). The mixture was sonicated, and the lysed cells were cleared by centrifugation at 16,000 rpm for 35 min. The supernatant was then incubated for 1 hr with glutathione Sepharose beads (GE Healthcare). After washing with 10 column volumes (CV) of lysis buffer followed by 10 CV of wash buffer (25 mM sodium phosphate [pH 8.0], 300 mM NaCl), the bound GST-fusion proteins were eluted in 10 CV of elution buffer (25 mM sodium phosphate [pH 8.0], 150 mM NaCl, 30 mM glutathione). Peak fractions were pooled and dialyzed with dialysis buffer (25 mM sodium phosphate [pH 7.0], 150 mM NaCl).

In Vitro Ubiquitin-Binding Assay

Equal amounts (10 μg) of purified GST-UBZ fusion proteins or GST protein alone were incubated with 10 μl of ubiquitin agarose (Boston Biochem) in binding buffer (25 mM HEPES [pH 7.9], 150 mM NaCl, 20 μM ZnCl2, 0.1% Tween 20, 5 mM β-mercaptoethanol) at 4°C for 1 hr. After washing with binding buffer four times, beads were boiled in SDS gel loading buffer, and the samples were analyzed by Coomassie blue staining.

GST Pull-Down Assay

Glutathione Sepharose beads (GE Health) with 10 μg of purified GST-UBZ fusion proteins or GST protein alone were incubated with different amounts of K63- or K48- linked polyubiquitin substrates (Boston Biochem) in binding buffer (described above) at 4°C overnight. Because the K63-linked polyubiquitin substrate contains a higher proportion of long chains than the K48-linked substrate, we used 10 μg of K48-linked polyubiquitin and 0.4 μg of K63-linked polyubiquitin in reactions of Figure 2C. This allows the level of K48-linked long chains to be comparable to that of the K63-linked long chains. In Figures 2E and 2F, 7 μg of K63-linked ubiquitin and 10 μg of K48-linked ubiquitin were used, respectively. After washing with the binding buffer four times, beads were boiled in SDS gel loading buffer and the samples were analyzed by immunoblotting.

Gel Filtration, Immunoprecipitation, and Protein Identification

We followed the protocol as described (Yan et al., 2010). Briefly, we fractionated HeLa nuclear extract by Superose 6 gel filtration chromatography, pooled the peak fractions containing FANCA, and immunoprecipitated the core complex with a FANCA antibody. The eluted immunoprecipitates were subjected to silver staining, mass spectrometry, and immunoblotting analyses.

Detailed experimental materials and methods can be found in the Supplemental Information.

ACCESSION NUMBERS

The NCBI accession number for the FAAP20 sequence reported in this paper is NP_872339.2 (C1orf86 isoform 2).

SUPPLEMENTAL INFORMATION

Supplemental Information includes six figures, Supplemental Experimental Procedures, and Supplemental References and can be found with this article online at doi:10.1016/j.molcel.2012.05.026.

ACKNOWLEDGMENTS

We thank Drs. D. Durocher, M. Huen, and A.R. Meetei for reagents, and Dr. David Schlessinger for critical reading of the manuscript. This work was supported in part by the Intramural Research Program of the National Institute on Aging (AG000688-07), National Institutes of Health.

Received: November 18, 2011
Revised: May 1, 2012
Accepted: May 17, 2012
Published online: June 14, 2012

REFERENCES

Al-Hakim, A., Escribano-Diaz, C., Landry, M.C., O'Donnell, L., Panier, S., Szilard, R.K., and Durocher, D. (2010). The ubiquitous role of ubiquitin in the DNA damage response. DNA Repair (Amst.) *9*, 1229–1240.

Ali, A.M., Pradhan, A., Singh, T.R., Du, C., Li, J., Wahengbam, K., Grassman, E., Auerbach, A.D., Pang, Q., and Meetei, A.R. (2012). FAAP20: a novel ubiquitin-binding FA nuclear core complex protein required for functional integrity of the FA-BRCA DNA repair pathway. Blood *119*, 3285–3294.

Ben-Yehoyada, M., Wang, L.C., Kozekov, I.D., Rizzo, C.J., Gottesman, M.E., and Gautier, J. (2009). Checkpoint signaling from a single DNA interstrand crosslink. Mol. Cell *35*, 704–715.

Bomar, M.G., Pai, M.T., Tzeng, S.R., Li, S.S., and Zhou, P. (2007). Structure of the ubiquitin-binding zinc finger domain of human DNA Y-polymerase eta. EMBO Rep. *8*, 247–251.

Chiu, R.K., Brun, J., Ramaekers, C., Theys, J., Weng, L., Lambin, P., Gray, D.A., and Wouters, B.G. (2006). Lysine 63-polyubiquitination guards against translesion synthesis-induced mutations. PLoS Genet. *2*, e116. 10.1371/journal.pgen.0020116.

Collins, N.B., Wilson, J.B., Bush, T., Thomashevski, A., Roberts, K.J., Jones, N.J., and Kupfer, G.M. (2009). ATR-dependent phosphorylation of FANCA on serine 1449 after DNA damage is important for FA pathway function. Blood *113*, 2181–2190.

Collis, S.J., Ciccia, A., Deans, A.J., Horejsi, Z., Martin, J.S., Maslen, S.L., Skehel, J.M., Elledge, S.J., West, S.C., and Boulton, S.J. (2008). FANCM and FAAP24 function in ATR-mediated checkpoint signaling independently of the fanconi anemia core complex. Mol. Cell *32*, 313–324.

Cordier, F., Grubisha, O., Traincard, F., Veron, M., Delepierre, M., and Agou, F. (2009). The zinc finger of NEMO is a functional ubiquitin-binding domain. J. Biol. Chem. *284*, 2902–2907.

Feng, L., and Chen, J. (2012). The E3 ligase RNF8 regulates KU80 removal and NHEJ repair. Nat. Struct. Mol. Biol. *19*, 201–206.

Garcia-Higuera, I., Taniguchi, T., Ganesan, S., Meyn, M.S., Timmers, C., Hejna, J., Grompe, M., and D'Andrea, A.D. (2001). Interaction of the Fanconi anemia proteins and BRCA1 in a common pathway. Mol. Cell *7*, 249–262.

Huang, M., Kim, J.M., Shiotani, B., Yang, K., Zou, L., and D'Andrea, A.D. (2010). The FANCM/FAAP24 complex is required for the DNA interstrand crosslink-induced checkpoint response. Mol. Cell *39*, 259–268.

Huen, M.S., Grant, R., Manke, I., Minn, K., Yu, X., Yaffe, M.B., and Chen, J. (2007). RNF8 transduces the DNA-damage signal via histone ubiquitylation and checkpoint protein assembly. Cell *131*, 901–914.

Kim, H., Yang, K., Dejsuphong, D., and D'Andrea, A.D. (2012). Regulation of Rev1 by the Fanconi anemia core complex. Nat. Struct. Mol. Biol. *19*, 164–170.

Knipscheer, P., Raschle, M., Smogorzewska, A., Enoiu, M., Ho, T.V., Scharer, O.D., Elledge, S.J., and Walter, J.C. (2009). The Fanconi anemia pathway promotes replication-dependent DNA interstrand cross-link repair. Science *326*, 1698–1701.

Kolas, N.K., Chapman, J.R., Nakada, S., Ylanko, J., Chahwan, R., Sweeney, F.D., Panier, S., Mendez, M., Wildenhain, J., Thomson, T.M., et al. (2007). Orchestration of the DNA-damage response by the RNF8 ubiquitin ligase. Science *318*, 1637–1640.

Kratz, K., Schopf, B., Kaden, S., Sendoel, A., Eberhard, R., Lademann, C., Cannavo, E., Sartori, A.A., Hengartner, M.O., and Jiricny, J. (2010). Deficiency of FANCD2-associated nuclease KIAA1018/FAN1 sensitizes cells to interstrand crosslinking agents. Cell *142*, 77–88.

Leung, J.W., Wang, Y., Fong, K.W., Huen, M.S., Li, L., and Chen, J. (2012). Fanconi anemia (FA) binding protein FAAP20 stabilizes FA complementation group A (FANCA) and participates in interstrand cross-link repair. Proc. Natl. Acad. Sci. USA *109*, 4491–4496.

Liu, T., Ghosal, G., Yuan, J., Chen, J., and Huang, J. (2010). FAN1 acts with FANCI-FANCD2 to promote DNA interstrand cross-link repair. Science *329*, 693–696.

Lok, G.T., Sy, S.M., Dong, S.S., Ching, Y.P., Tsao, S.W., Thomson, T.M., and Huen, M.S. (2011). Differential regulation of RNF8-mediated Lys48- and Lys63-based poly-ubiquitylation. Nucleic Acids Res. *40*, 196–205.

MacKay, C., Declais, A.C., Lundin, C., Agostinho, A., Deans, A.J., MacArtney, T.J., Hofmann, K., Gartner, A., West, S.C., Helleday, T., et al. (2010). Identification of KIAA1018/FAN1, a DNA repair nuclease recruited to DNA damage by monoubiquitinated FANCD2. Cell *142*, 65–76.

Mailand, N., Bekker-Jensen, S., Faustrup, H., Melander, F., Bartek, J., Lukas, C., and Lukas, J. (2007). RNF8 ubiquitylates histones at DNA double-strand breaks and promotes assembly of repair proteins. Cell *131*, 887–900.

Marteijn, J.A., Bekker-Jensen, S., Mailand, N., Lans, H., Schwertman, P., Gourdin, A.M., Dantuma, N.P., Lukas, J., and Vermeulen, W. (2009). Nucleotide excision repair-induced H2A ubiquitination is dependent on MDC1 and RNF8 and reveals a universal DNA damage response. J. Cell Biol. *186*, 835–847.

Meetei, A.R., Sechi, S., Wallisch, M., Yang, D., Young, M.K., Joenje, H., Hoatlin, M.E., and Wang, W. (2003). A multiprotein nuclear complex connects Fanconi anemia and Bloom syndrome. Mol. Cell. Biol. *23*, 3417–3426.

Muniandy, P.A., Liu, J., Majumdar, A., Liu, S.T., and Seidman, M.M. (2010). DNA interstrand crosslink repair in mammalian cells: step by step. Crit. Rev. Biochem. Mol. Biol. *45*, 23–49.

Muniandy, P.A., Thapa, D., Thazhathveetil, A.K., Liu, S.T., and Seidman, M.M. (2009). Repair of laser-localized DNA interstrand cross-links in G1 phase mammalian cells. J. Biol. Chem. *284*, 27908–27917.

Nam, E.A., and Cortez, D. (2011). ATR signalling: more than meeting at the fork. Biochem. J. *436*, 527–536.

Shen, X., Do, H., Li, Y., Chung, W.-Y., Tomasz, M., de Winter, J.P., Xia, B., Elledge, S.J., Wang, W., and Li, L. (2009). Recruitment of Fanconi anemia and breast cancer proteins to DNA damage sites is differentially governed by replication. Mol. Cell *35*, 716–723.

Singh, T.R., Saro, D., Ali, A.M., Zheng, X.F., Du, C.H., Killen, M.W., Sachpatzidis, A., Wahengbam, K., Pierce, A.J., Xiong, Y., et al. (2010). MHF1-MHF2, a histone-fold-containing protein complex, participates in the Fanconi anemia pathway via FANCM. Mol. Cell *37*, 879–886.

Smogorzewska, A., Desetty, R., Saito, T.T., Schlabach, M., Lach, F.P., Sowa, M.E., Clark, A.B., Kunkel, T.A., Harper, J.W., Colaiacovo, M.P., et al. (2010). A genetic screen identifies FAN1, a Fanconi anemia-associated nuclease necessary for DNA interstrand crosslink repair. Mol. Cell *39*, 36–47.

Sy, S.M., Jiang, J., Dong, S.S., Lok, G.T., Wu, J., Cai, H., Yeung, E.S., Huang, J., Chen, J., Deng, Y., et al. (2011). Critical roles of ring finger protein RNF8 in replication stress responses. J. Biol. Chem. *286*, 22355–22361.

Takata, M., Ishiai, M., and Kitao, H. (2009). The Fanconi anemia pathway: insights from somatic cell genetics using DT40 cell line. Mutat. Res. *668*, 92–102.

Ulrich, H.D., and Walden, H. (2010). Ubiquitin signalling in DNA replication and repair. Nat. Rev. Mol. Cell Biol. *11*, 479–489.

Wang, B., and Elledge, S.J. (2007). Ubc13/Rnf8 ubiquitin ligases control foci formation of the Rap80/Abraxas/Brca1/Brcc36 complex in response to DNA damage. Proc. Natl. Acad. Sci. USA *104*, 20759–20763.

Wang, W. (2007). Emergence of a DNA-damage response network consisting of Fanconi anaemia and BRCA proteins. Nat. Rev. Genet. *8*, 735–748.

Wang, X., Kennedy, R.D., Ray, K., Stuckert, P., Ellenberger, T., and D'Andrea, A.D. (2007). Chk1-mediated phosphorylation of FANCE is required for the Fanconi anemia/BRCA pathway. Mol. Cell. Biol. *27*, 3098–3108.

Wen, Q., Scorah, J., Phear, G., Rodgers, G., Rodgers, S., and Meuth, M. (2008). A mutant allele of MRE11 found in mismatch repair-deficient tumor cells suppresses the cellular response to DNA replication fork stress in a dominant negative manner. Mol. Biol. Cell *19*, 1693–1705.

Yamamoto, K.N., Kobayashi, S., Tsuda, M., Kurumizaka, H., Takata, M., Kono, K., Jiricny, J., Takeda, S., and Hirota, K. (2011). Involvement of SLX4 in interstrand cross-link repair is regulated by the Fanconi anemia pathway. Proc. Natl. Acad. Sci. USA *108*, 6492–6496.

Yan, Z., Delannoy, M., Ling, C., Daee, D., Osman, F., Muniandy, P.A., Shen, X., Oostra, A.B., Du, H., Steltenpool, J., et al. (2010). A histone-fold complex and FANCM form a conserved DNA-remodeling complex to maintain genome stability. Mol. Cell *37*, 865–878.

Zhao, G.Y., Sonoda, E., Barber, L.J., Oka, H., Murakawa, Y., Yamada, K., Ikura, T., Wang, X., Kobayashi, M., Yamamoto, K., et al. (2007). A critical role for the ubiquitin-conjugating enzyme Ubc13 in initiating homologous recombination. Mol. Cell *25*, 663–675.

Extensive gene deletions in Japanese patients with Diamond-Blackfan anemia

Madoka Kuramitsu,[1] Aiko Sato-Otsubo,[2] Tomohiro Morio,[3] Masatoshi Takagi,[3] Tsutomu Toki,[4] Kiminori Terui,[4] RuNan Wang,[4] Hitoshi Kanno,[5] Shouichi Ohga,[6] Akira Ohara,[7] Seiji Kojima,[8] Toshiyuki Kitoh,[9] Kumiko Goi,[10] Kazuko Kudo,[11] Tadashi Matsubayashi,[12] Nobuo Mizue,[13] Michio Ozeki,[14] Atsuko Masumi,[1] Haruka Momose,[1] Kazuya Takizawa,[1] Takuo Mizukami,[1] Kazunari Yamaguchi,[1] Seishi Ogawa,[2] Etsuro Ito,[4] and Isao Hamaguchi[1]

[1]Department of Safety Research on Blood and Biological Products, National Institute of Infectious Diseases, Tokyo, Japan; [2]Cancer Genomics Project, Graduate School of Medicine, The University of Tokyo, Tokyo, Japan; [3]Department of Pediatrics and Developmental Biology, Graduate School of Medicine, Tokyo Medical and Dental University, Bunkyo-ku, Tokyo, Japan; [4]Department of Pediatrics, Hirosaki University Graduate School of Medicine, Hirosaki, Japan; [5]Department of Transfusion Medicine and Cell Processing, Tokyo Women's Medical University, Tokyo, Japan; [6]Department of Pediatrics, Graduate School of Medical Sciences, Kyushu University, Fukuoka, Japan; [7]First Department of Pediatrics, Toho University School of Medicine, Tokyo, Japan; [8]Department of Pediatrics, Nagoya University Graduate School of Medicine, Nagoya, Japan; [9]Department of Hematology/Oncology, Shiga Medical Center for Children, Shiga, Japan; [10]Department of Pediatrics, School of Medicine, University of Yamanashi, Yamanashi, Japan; [11]Division of Hematology and Oncology, Shizuoka Children's Hospital, Shizuoka, Japan; [12]Department of Pediatrics, Seirei Hamamatsu General Hospital, Shizuoka, Japan; [13]Department of Pediatrics, Kushiro City General Hospital, Hokkaido, Japan; and [14]Department of Pediatrics, Graduate School of Medicine, Gifu University, Gifu, Japan

Fifty percent of Diamond-Blackfan anemia (DBA) patients possess mutations in genes coding for ribosomal proteins (RPs). To identify new mutations, we investigated large deletions in the RP genes *RPL5*, *RPL11*, *RPL35A*, *RPS7*, *RPS10*, *RPS17*, *RPS19*, *RPS24*, and *RPS26*. We developed an easy method based on quantitative-PCR in which the threshold cycle correlates to gene copy number. Using this approach, we were able to diagnose 7 of 27 Japanese patients (25.9%) possessing mutations that were not detected by sequencing. Among these large deletions, similar results were obtained with 6 of 7 patients screened with a single nucleotide polymorphism array. We found an extensive intragenic deletion in *RPS19*, including exons 1-3. We also found 1 proband with an *RPL5* deletion, 1 patient with an *RPL35A* deletion, 3 with *RPS17* deletions, and 1 with an *RPS19* deletion. In particular, the large deletions in the *RPL5* and *RPS17* alleles are novel. All patients with a large deletion had a growth retardation phenotype. Our data suggest that large deletions in RP genes comprise a sizable fraction of DBA patients in Japan. In addition, our novel approach may become a useful tool for screening gene copy numbers of known DBA genes. (*Blood*. 2012;119(10): 2376-2384)

Introduction

Diamond-Blackfan anemia (DBA; MIN# 105650) is a rare congenital anemia that belongs to the inherited BM failure syndromes, generally presenting in the first year of life. Patients typically present with a decreased number of erythroid progenitors in their BM.[1] A main feature of the disease is red cell aplasia, but approximately half of patients show growth retardation and congenital malformations in the craniofacial, upper limb, cardiac, and urinary systems. Predisposition to cancer, in particular acute myeloid leukemia and osteogenic sarcoma, is also characteristic of the disease.[2]

Mutations in the *RPS19* gene were first reported in 25% of DBA patients by Draptchinskaia et al in 1999.[3] Since that initial finding, many genes that encode large (RPL) or small (RPS) ribosomal subunit proteins were found to be mutated in DBA patients, including *RPL5* (approximately 21%), *RPL11* (approximately 9.3%), *RPL35A* (3.5%), *RPS7* (1%), *RPS10* (6.4%), *RPS17* (1%), *RPS24* (2%), and *RPS26* (2.6%).[4-7] To date, approximately half of the DBA patients analyzed have had a mutation in one of these genes. Konno et al screened 49 Japanese patients and found that 30% (12 of 49) carried mutations.[8] In addition, our data showed that 22 of 68 DBA patients (32.4%) harbored a mutation in ribosomal protein (RP) genes (T.T., K.T., R.W., and E.I., unpublished observation, April 16, 2011). These abnormalities of RP genes cause defects in ribosomal RNA processing, formation of either the large or small ribosome subunit, and decreased levels of polysome formation,[4-6,9-12] which is thought to be one of the mechanisms for impairment of erythroid lineage differentiation.

Although sequence analyses of genes responsible for DBA are well established and have been used to identify new mutations, it is estimated that approximately half of the mutations remain to be determined. Because of the difficulty of investigating whole allele deletions, there have been few reports regarding allelic loss in DBA, and they have only been reported for *RPS19* and *RPL35A*.[3,6,13] However, a certain percentage of DBA patients are thought to have a large deletion in RP genes. Therefore, a detailed analysis of allelic loss mutations should be conducted to determine other RP genes that might be responsible for DBA.

In the present study, we investigated large deletions using our novel approach for gene copy number variation analysis based on quantitative-PCR and a single nucleotide polymorphism (SNP) array. We screened Japanese DBA patients and found 7 patients with a large deletion in an allele in *RPL5*, *RPL35A*, *RPS17*, or *RPS19*. Interestingly, all of these patients with a large deletion had a phenotype of growth retardation, including short stature and

Submitted July 24, 2011; accepted November 15, 2011. Prepublished online as *Blood* First Edition paper, January 18, 2012; DOI 10.1182/blood-2011-07-368662.

The online version of this article contains a data supplement.

The publication costs of this article were defrayed in part by page charge payment. Therefore, and solely to indicate this fact, this article is hereby marked "advertisement" in accordance with 18 USC section 1734.

Table 1. Primers used for synchronized quantitative-PCR (s-q-PCR) of RPL proteins

Gene	Primer name	Sequence	Primer name	Sequence	Size, bp
RPL5	L5-02F	CTCCCAAAGTGCTTGAGATTACAG	L5-02R	CACCTTTTCCTAACAAATTCCCAAT	132
	L5-05F	AGCCCTCCAACCTAGGTGACA	L5-05R	GAATTGGGATGGGCAAGAACT	102
	L5-17F	TGAACCCTTGCCCTAAAACATG	L5-17R	TCTTGGTCAGGCCCTGCTTA	105
	L5-19F	ATTGTGCAAACTCGATCACTAGCT	L5-19R	GTGTCTGAGGCTAACACATTTCCAT	103
	L5-21F	GTGCCACTCTCTTGGACAAACTG	L5-21R	CATAGGGCCAAAAGTCAAATAGAAG	102
	L5-28F	TCCACTTTAGGTAGGCGAAACC	L5-28R	TCAGATTTGGCATGTACCTTTCA	102
RPL11	L11-06F	GCACCCACATGGCTTAAAGG	L11-6R	CAACCAACCCATAGGCCAAA	102
	L11-20F	GAGCCCCCTTTCTCAGATGATA	L11-20R	CATGAACTTGGGCTCTGAATCC	109
	L11-22F	TATGTGCAGATAAGAGGGCAGTCT	L11-22R	ATACAGATAAGGAAACTGAGGCAGATT	98
RPL19	L19-02F	TGGCCTCTCATAAAGGAAATCTCT	L19-02R	GGAATGCAGGCAAGTTACTCTGTT	103
	L19-08F	TTTGAAGGCAAGAAATAAGTTCCA	L19-08R	AGCACATCACAGAGTCCAAATAGG	107
	L19-16F	GGTTAGTTGAAGCAGGAGCCTTT	L19-16R	TGCTAGGGAGACAGAAGCACATC	102
	L19-19F	GGACCAGTAGTTGTGACATCAGTTAAG	L19-19R	CCCATTTGTAACCCCCACTTG	106
RPL26	L26-03F	TCCAAAGAGCTGAGACAGAAGTACA	L26-03R	TCCATCAAGACAACGAGAACAAGT	102
	L26-16F	TTTGAGAATGCTTGAGAGAAGGAA	L26-16R	TTCCAGCACATGTAAAATCAAGGA	102
	L26-18F	ATGTTTTAATAAGCCCTCCAGTTGA	L26-18R	GAGAACAGCAAGTTGAAAGGTTCA	102
	L26-20F	GGGCTTTGCTTGATCACTCTAGA	L26-20R	AGGGAGCCCGAAAACATTTAC	104
RPL35A	L35A-01F	TGTGGCTTCTATTTTGCGTCAT	L35A-01R	GGAATTACCTCCTTTATTGCTTACAAG	121
	L35A-07F	TTTCCGTTCTGTCTATTGCTGTGT	L35A-07R	GAACCCTGAGTGGAGGATGTTC	113
	L35A-17F	GCCCACAACCTCCAGAGAATC	L35A-17R	GGATCACTTGAGGCCAGGAAT	104
	L35A-18F	TTAGGTGGGCTTTTCAGTCTCAA	L35A-18R	ATCTCCTGATTCCCCAACTTTGT	102
RPL36	L36-02F	CCGCTCTACAAGTGAAGAAATTCTG	L36-02R	CTCCCTCTGCCTGTGAAATGA	102
	L36-04F	TGCGTCCTGCCAGTGTTG	L36-04R	GGGTAGCTGTGAGAACCAAGGT	105
	L36-17F	CCCCTTGAAAGGACAGCAGTT	L36-17R	TTGGACACCAGGCACAGACTT	114

Table 2. Primers used for s-q-PCR of RPS proteins

Gene	Primer name	Sequence	Primer name	Sequence	Size, bps
RPS7	S7-11F	GCGCTGCCAGATAGGAAATC	S7-11R	TTAGGGAGCTGCCTTACATATGG	102
	S7-12F	ACTGGCAGTTCTGTGATGCTAAGT	S7-12R	ACTCTTGCTCATCTCCAAAACCA	102
	S7-16F	GTGTCTGTGCCAGAAAGCTTGA	S7-16R	GAACCATGCAAAAGTGCCAATAT	112
RPS10	S10-03F	CTACGGTTTTGTGTGGGTCACTT	S10-03R	CATCTGCAAGAAGGAGACGATTG	102
	S10-15F	GTTGGCCTGGAGTCGTGATTT	S10-15R	ATTCCAAGTGCACCATTTCCTT	101
	S10-17F	AATGGTGTTTAGGCCAACGTTAC	S10-17R	TTTGAACAGTGGTTTTTGTGCAT	100
RPS14	S14-03F	GAATTCCAAACCCTTCTGCAAA	S14-03R	TTGCTTCATTTACTCCTCAAGACATT	104
	S14-05F	ACAACCAGCCCTCTACCTCTTTT	S14-05R	GGAAGACGCCGGCATTATT	102
	S14-06F	CGCCTCTACCTCGCCAAAC	S14-06R	GGGATCGGTGCTATTGTTATTCC	102
	S14-09F	GCCATCATGCCGAAACATACT	S14-09R	AACGCGCCACAGGAGAGA	102
	S14-13F	ATCAGGTGGAGCACAGGAAAAC	S14-13R	GCGAGGGAGCTGCTTGATT	111
	S14-15F	AGAAGTTTTAGTGAGGCAGAAATGAGA	S14-15R	TCCCCTGGCTATTAAATGAAACC	102
	S14-19F	GATGAATTGTCCTTTCCTCCATTC	S14-19R	TAGGCGGAAACCAAAAATGCT	102
RPS15	S15-11F	CTCAGCTAATAAAGGCGCACATG	S15-11R	CCTCACACCACGAACCTGAAG	108
	S15-15F	GGTTGGAGAACATGGTGAGAACTA	S15-15R	CACATCCCTGGGCCACTCT	108
RPS17	S17-03F	ACTGCTGTCGTGGCTCGATT	S17-03R	GATGACCTGTTCTTCTGGCCTTA	121
	S17-05F	GAAAACAGATACAAATGGCATGGT	S17-05R	TGCCTCCCACTTTTCCAGAGT	114
	S17-12F	CTATGTGTAGGAGGTCCCAGGATAG	S17-12R	CCACCTGGTACTGAGCACATGT	102
	S17-16F	TAGCGGAAGTTGTGTGCATTG	S17-16R	CAAGAACAGAAGCAGCCAAGAG	102
	S17-18F	TGGCTGAATCTGCCTGCTT	S17-18R	GCCTTGTATGTACCTGGAAATGG	103
	S17-20F	GGGCCCTTCACAAATGTTGA	S17-20R	GCAAAACTCTGTCCCTTTGAGAA	101
RPS19	S19-24F	CCATCCCAAGAATGCACACA	S19-24R	CGCCGTAGCTGGTACTCATG	120
	S19-28F	GACACACCTGTTGAGTCCTCAGAGT	S19-28R	GCTTCTATTAACTGGAGCACACATCT	114
	S19-36F	CTCTTGAGGGTGGTCTGGAAAT	S19-36R	GTCTTTGCGGGTTCTTCCTCTAC	102
	S19-40F	GGAACGGTGTCAGGATTCAAG	S19-40R	AGCGGCTGTACACCAGAAATG	101
	S19-44F	CTGAGGTTGAGTGTCCCATTTCT	S19-44R	GCACCGGGCCTCTGTTATC	104
	S19-57F	CAGGGACACAGTGCTGAGAAACT	S19-57R	TGAGATGTCCCATTTTCACTATTGTT	101
	S19-58F	CATGATGTTAGCTCCGTTGCATA	S19-58R	ATTTTGGGAAGAGTGAAGCTTAGGT	102
	S19-62F	GCAACAGAGCGAGACTCCATTT	S19-62R	AGCACTTTTCGGCACTTACTTCA	102
	S19-65F	ACATTTCCCAGAGCTGACATGA	S19-65R	TCGGGACACCTAGACCTTGCT	102
RPS24	S24-17F	CGACCACGTCTGGCTTAGAGT	S24-17R	CCTTCATGCCCAACCAAGTC	101
	S24-20F	ACAAGTAAGCATCATCACCTCGAA	S24-20R	TTTCCCTCACAGCTATCGTATGG	105
	S24-32F	GGGAAATGCTGTGTCCACATACT	S24-32R	CTGGTTTCATGGCTCCAGAGA	105
RPS26	S26-03F	CGCAGCAGTCAGGGACATTT	S26-03R	AAGTTGGGCGAAGGCTTTAAG	104
	S26-05F	ATGGAGGCCGTCTAGTTTGGT	S26-05R	TGCCTACCCTGAACCTTGCT	102
RPS27A	S27A-09F	GCTGGAGTGCATTCGCTTGT	S27A-09R	CACGCCTGTAATCCCCACTAA	102
	S27A-12F	CAGGCTTGGTGTGCTGTGACT	S27A-12R	ACGTCCATCTTCCAGCTGCTT	103
	S27A-18F	GGGTTTTTCCTGTTTGGTATTTGA	S27A-18R	AAAGGCCAGCTTTGCAAGTG	111
	S27A-22F	TTACCATATTGCCAGTCTTTCCATT	S27A-22R	TTCATATGCATTTGCACAAACTGT	106

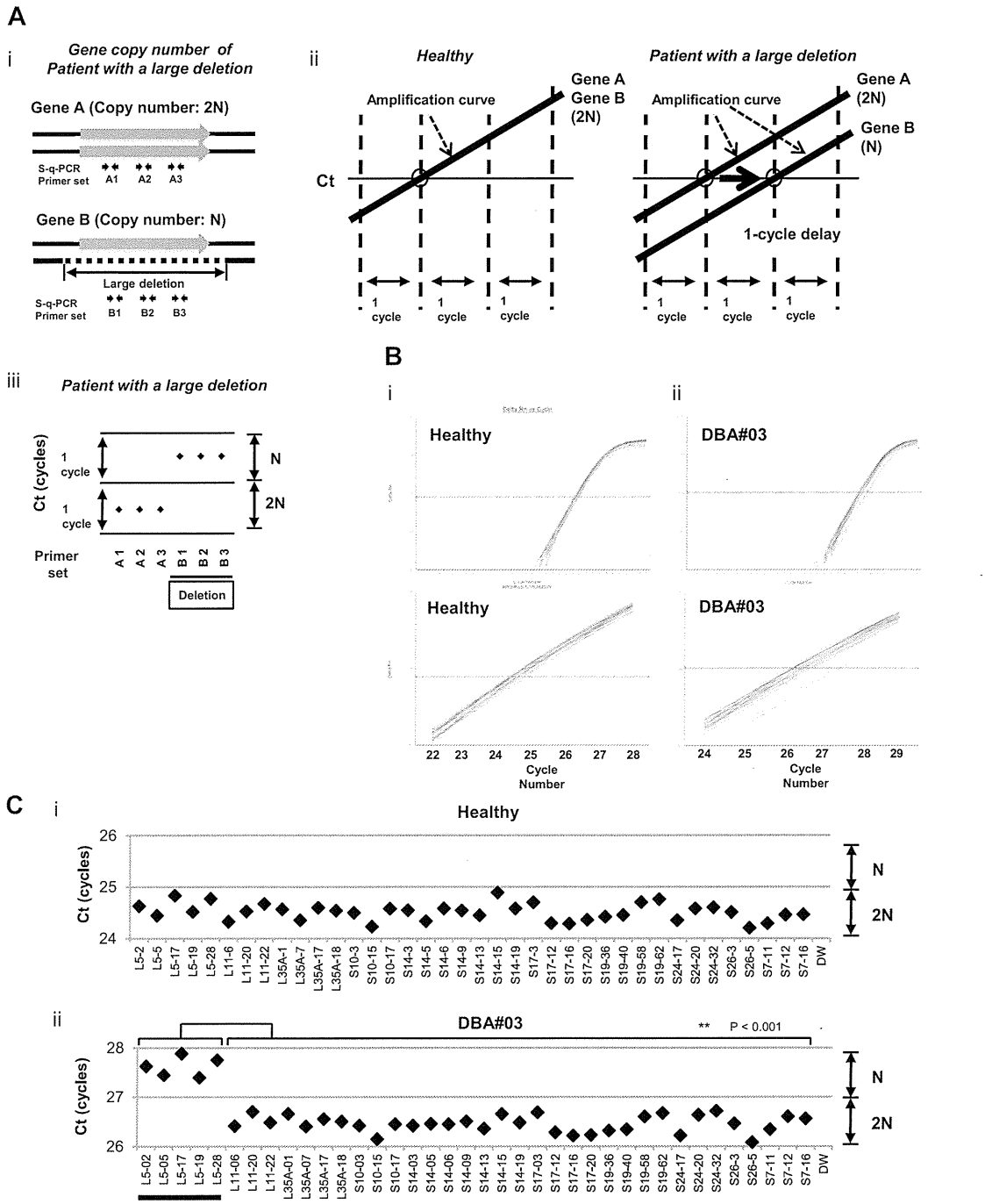

Figure 1. s-q-PCR can determine a large gene deletion in DBA. (A) Concept of the DBA s-q-PCR assay. The difference in gene copy number between a healthy sample and that with a large deletion is 2-fold (i). When all genomic s-q-PCR for genes of interest synchronously amplify DNA fragments, a 2-fold difference in the gene copy number is detected by a 1-cycle difference of the Ct scores of the s-q-PCR amplification curves (ii). Also shown is a dot plot of the Ct scores (iii). (B) Results of the amplification curves of s-q-PCR performed with a healthy person (i) and a DBA patient (patient 3; ii). The top panel shows the results of PCR cycles; the bottom panel is an extended graph of the PCR cycles at logarithmic amplification. (C) Graph showing Ct scores of s-q-PCR. If all specific primer sets for DBA genes show a 1-cycle delay relative to each other, this indicates a large deletion in the gene. Gene primer sets with a large deletion are underlined in the graph. $^{**}P < .001$.

small-for-gestational age (SGA), which suggests that this is a characteristic of DBA patients with a large gene deletion in Japan.

Methods

Patient samples

Genomic DNA was extracted using the GenElute Blood Genomic DNA Kit (Sigma-Aldrich) according to the manufacturer's protocol. Clinical manifestation of patients from a Japanese DBA genomic library are listed elsewhere or are as reported by Konno et al.[8] The study was approved by the institutional review board at the National Institute of Infectious Diseases and Hirosaki University.

DBA gene copy number assay by s-q-PCR

For s-q-PCR, primers were designed using Primer Express Version 3.0 software (Applied Biosystems). Primers are listed in Tables 1 and 2. Genomic DNA in water was denatured at 95°C for 5 minutes and

immediately cooled on ice. The composition of the s-q-PCR mixture was as follows: 5 ng of denatured genomic DNA, 0.4mM forward and reverse primers, 1× SYBR Premix Ex Taq II (Takara), and 1× ROX reference dye II (Takara) in a total volume of 20 μL (all experiments were performed in duplicate). Thermal cycling was performed using the Applied Biosystems 7500 fast real-time PCR system. Briefly, the PCR mixture was denatured at 95°C for 30 seconds, followed by 35 cycles of 95°C for 5 seconds, 60°C for 34 seconds, and then dissociation curve measurement. Threshold cycle (Ct) scores were determined as the average of duplicate samples. The technical errors of Ct scores in the triplicate analysis were within 0.2 cycles (supplemental Figure 1, available on the *Blood* Web site; see the Supplemental Materials link at the top of the online article). The sensitivity and specificity of this method was evaluated with 15 healthy samples. Any false positive was not observed in all primer sets in all healthy samples (supplemental Figure 2). We performed direct sequencing of the s-q-PCR products. The results of the sequence analysis were searched for using BLAST to confirm uniqueness. Sequence data were obtained from GenBank (http://www.ncbi.nlm.nih.gov/gene/) and Ensemble Genome Browser (http://uswest.ensembl.org).

Genomic PCR

Genomic PCR was performed using KOD FX (Toyobo) according to the manufacturer's step-down PCR protocol. Briefly, the PCR mixture contained 20 ng of genomic DNA, 0.4mM forward and reverse primers, 1mM dNTP, 1× KOD FX buffer, and 0.5 U KOD FX in a total volume of 25 μL in duplicate. Primers are given in supplemental Figure 3 and Table 2. PCR mixtures were denatured at 94°C for 2 minutes, followed by 4 cycles of 98°C for 10 seconds, 74°C for 12 minutes, followed by 4 cycles of 98°C for 10 seconds, 72°C for 12 minutes followed by 4 cycles of 98°C for 10 seconds, 70°C for 12 minutes, followed by 23 cycles of 98°C for 10 seconds and 68°C for 12 minutes. PCR products were loaded on 0.8% agarose gels and detected by LAS-3000 (Fujifilm).

DNA sequencing analysis

The genomic PCR product was purified by the GenElute PCR clean-up kit (Sigma-Aldrich) according to the manufacturer's instructions. Direct sequencing was performed using the BigDye Version 3 sequencing kit. Sequences were read and analyzed using a 3120x genetic analyzer (Applied Biosystems).

SNP array-based copy number analysis

SNP array experiments were performed according to the standard protocol of GeneChip Human Mapping 250K Nsp arrays (Affymetrix). Microarray data were analyzed for determination of the allelic-specific copy number using the CNAG program, as described previously.[14] All microarray data are available at the EGA database (www.ebi.ac.uk/ega) under accession number EGAS00000000105.

Results

Construction of a convenient method for RP gene copy number analysis based on s-q-PCR

We focused on the heterozygous large deletions in DBA-responsible gene. The difference in copy number of genes between a mutated DBA allele and the intact allele was 2-fold (N and 2N; Figure 1Ai). If each PCR can synchronously amplify DNA fragments when the template genomic DNA used is of normal karyotype, it is possible to conveniently detect a gene deletion with a 1-cycle delay in s-q-PCR analysis (Figure 1Aii-iii).

Table 3. Summary of mutations and the mutation rate observed in Japanese DBA patients

Gene	Sequencing analysis
RPS19	10
RPL5	6
RPL11	3
RPS17	1
RPS10	1
RPS26	1
RPL35A	0
RPS24	0
RPS14	0
Mutations, n (%)	22 (32.4%)
Total analyzed, N	68

To apply this strategy for allelic analysis of DBA, we prepared primers for 16 target genes, *RPL5*, *RPL11*, *RPL35A*, *RPS10*, *RPS19*, *RPS26*, *RPS7*, *RPS17*, *RPS24*, *RPL9*, *RPL19*, *RPL26*, *RPL36*, *RPS14*, *RPS15*, and *RPS27A*, under conditions in which the Ct of s-q-PCR would occur within 1 cycle of that of the other primer sets (Tables 1 and 2). At the same time, we defined the criteria of a large deletion in our assay as follows. If multiple primer sets for one gene showed a 1-cycle delay from the other gene-specific primer set at the Ct score, we assumed that this represented a large deletion. As shown in Figure 1Bii and 1Cii, the specific primer sets for *RPL5* (L5-02, L5-05, L5-17, L5-19, and L5-28) detected a 1-cycle delay with respect to the mutated allele of patient 3. This assessment could be verified by simply confirming the difference of the cycles with the s-q-PCR amplification curves.

Study of large gene deletions in a Japanese DBA genomic DNA library

Sixty-eight Japanese DBA patients were registered and blood genomic DNA was collected at Hirosaki University. All samples were first screened for mutations in *RPL5*, *L11*, *L35A*, *S10*, *S14*, *S17*, *S19*, and *S26* by sequencing. Among these patients, 32.4% (22 of 68) had specific DBA mutations (Table 3 and data not shown). We then screened for large gene deletions in 27 patients from the remaining 46 patients who did not possess mutations as determined by sequencing (Table 4).

When we performed the s-q-PCR DBA gene copy number assay, 7 of 27 samples displayed a 1-cycle delay of Ct scores: 1 patient had *RPL5* (patient 14), 1 had *RPL35A* (patient 71), 3 had *RPS17* (patients 3, 60, 62), and 2 had *RPS19* (patients 24 and 72; Figure 2 and Table 4). Among these patients, the large deletions in the *RPL5* and *RPS17* genes are the first reported cases of allelic deletions in DBA. From these results, we estimate that a sizable number of Japanese DBA patients have a large deletion.

Based on our findings, the rate of large deletions was approximately 25.9% (7 of 27) in a category of unspecified gene mutations. Such mutations have typically gone undetected by conventional sequence analysis. We could not find any additional gene deletions in the analyzed samples.

Confirmation of the gene copy number for DBA genes by genome-wide SNP array

We performed genome-wide copy number analysis of the 27 DBA patients with a SNP array to confirm our s-q-PCR results. SNP array showed that patient 3 had a large deletion in

Table 4. Characteristics of DBA patients tested

Patient no.	Age at diagnosis	Sex	Hb, g/dL	Large deletion by s-q-PCR	Large deletion by SNP array	Inheritance	Malformations	Response to first steroid therapy
Patients with a large deletion in RP genes								
3*†	1 y	M		RPL5	RPL5	Sporadic	Short stature, thumb anomalies	Response
14*	5 y	M	5.5	RPS17	RPS17	Sporadic	White spots, short stature	Response
24*†	1 mo	F	5.5	RPS19	ND	Sporadic	Short stature, SGA	Response
60*†	2 mo	F	2.4	RPS17	RPS17	Sporadic	SGA	NT
62*†	1 mo	F	6.2	RPS17	RPS17	Sporadic	Small ASD, short stature, SGA	Response
71	0 y	M	5.3	RPL35A	RPL35A	Sporadic	Thumb anomalies, synostosis of radius and ulna, Cohelia Lange-like face, cleft palate, underdescended testis, short stature, cerebellar hypoplasia, fetal hydrops	NT
72†	0 y	M	2	RPS19	RPS19	Sporadic	Thumb anomalies, flat thenar, testicular hypoplasia, fetal hydrops, short stature, learning disability	No
Patients without a large deletion in RP genes								
5*	1 y	F	3.1	ND	ND	Sporadic	ND	Response
15*	1 mo	F	1.6	ND	ND	Sporadic	ND	Response
21*	1 y	F	2.6	ND	ND	Sporadic	ND	Response
26*	1 y 1 mo	F	8	ND	ND	Sporadic	Congenital hip dislocation, spastic quadriplegia, hypertelorism, nystagmus, short stature, learning disability	Response
33*	2 mo	F	1.3	ND	ND	Sporadic	ND	Response
36*	0 y	M	8.2	ND	ND	Familial	ND	Response
37*	4 y	M	6.1	ND	ND	Sporadic	Hypospadias, underdescended testis, SGA	NT
45*	5 d	M	5.1	ND	ND	Sporadic	Short stature, microcephaly, mental retardation, hypogammaglobulinemia	Poor
50*	2 m	F	3.4	ND	ND	Familial	ND	Response
61*	9 m	M	4	ND	ND	Sporadic	ND	Response
63*	0 y	M	6.8	ND	ND	Sporadic	Micrognathia, hypertelorism, short stature	Response
68	1 y 4 mo	M	5.9	ND	ND	Sporadic	ND	NT (CR)
69	1 y	M	9.3	ND	ND	Sporadic	ND	Response
76	0 y	M	4	ND	ND	Sporadic	ND	Response
77	0 y	M	7.8	ND	ND	Familial	Short stature	No
83	9 mo	F	3	ND	ND	Sporadic	ND	NT
90	10 mo	M	9	ND	ND	Sporadic	ND	No
91	0 y	F	3.8	ND	ND	Sporadic	ND	Response
92	2 mo	M	3.7	ND	ND	Sporadic	ASD, PFO, melanosis, underdescended testis, SGA, short stature	Response
93	11 mo	M	2.2	ND	ND	Sporadic	White spots, senile face, corneal opacity, underdescended testis, syndactyly, ectrodactyly, flexion contracture, extension contracture	Response

ND indicates not detected; NT, not tested; CR, complete remission; ASD, atrial septal defect; and PFO, persistent foramen ovale.

*Status data of Japanese probands 3 to 63 is from a report by Konno et al.[8]

†Large deletions of the parents of 5 DBA patients (3, 24, 60, 62, and 72) were analyzed by s-q-PCR, but there were no deletions in DBA genes in any of the 5 pairs of parents.

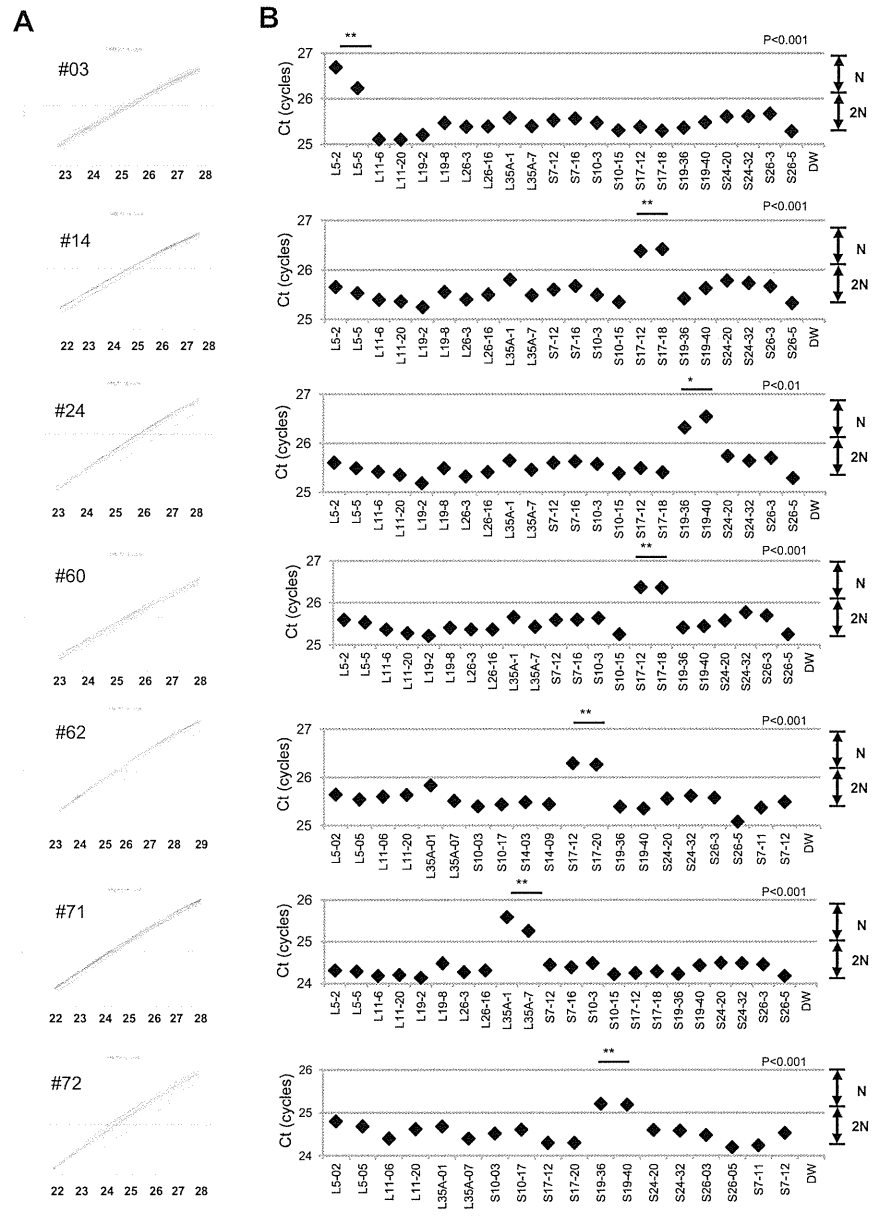

Figure 2. Detection of 7 mutations with a large deletion in DBA patients. Genomic DNA of 27 Japanese DBA patients with unknown mutations were subjected to the DBA gene copy number assay. (A) Amplification curve of s-q-PCR of a mutation with a large deletion. The deleted gene can be easily distinguished. (B) Ct score (cycles) of representative s-q-PCR with DBA genomic s-q-PCR primers. Results of the 2 gene-specific primer pairs indicated in the graph are representative of at least 2 sets for each gene-specific primer (carried out in the same run). $^{**}P < .001$; $^{*}P < .01$

chromosome 1 (ch1) spanning 858 kb (Figure 3A); patient 71 had a large deletion in ch3 spanning 786 kb (Figure 3B); patients 14, 60, and 62 had a large deletion in ch15 spanning 270 kb, 260 kb, and 330 kb, respectively (Figure 3C); and patient 72 had a large deletion in ch19 spanning 824 kb (Figure 3D). However, there were no deletions detected in ch19 in patient 24 (Figure 3D). Genes estimated to reside within a large deletion are listed in supplemental Table 1. Consistent with these s-q-PCR results, 6 of 7 large deletions were detected and confirmed as deleted regions, and these large deletions contained *RPL5*, *RPL35A*, *RPS17*, and *RPS19* (Table 4 and supplemental Table 1). Other large deletions in RP genes were not detected by this analysis. From these results, we conclude that the synchronized multiple PCR amplification method has a detection sensitivity comparable to that of SNP arrays.

Detailed examination of a patient with intragenic deletion in the RPS19 allele (patient 24)

Interestingly, for patient 24, in whom we could not detect a large deletion by SNP array at s-q-PCR gene copy number analysis, 2 primer sets for *RPS19* showed a 1-cycle delay (RPS19-36 and RPS19-40), but 2 other primer pairs (RPS19-58 and RPS19-62) did not show this delay (Figure 4A). We attempted to determine the deleted region in detail by testing more primer sets on *RPS19*. We tested a total of 9 primer sets for *RPS19* (Figure 4B) and examined the gene copy numbers. Surprisingly, 4 primer sets (S19-24, S19-36, S19-40, and S19-44) for intron 3 of *RPS19* indicated a 1-cycle delay, but the other primers for *RPS19* located on the 5′untranslated region (5′UTR), intron 3, or 3′UTR did not show this delay (S19-57, S19-58, S19-28, S19-62, and S19-65; Figure 4B-C). These results suggest that the intragenic deletion occurred in the *RPS19* allele. To confirm this deleted region precisely, we performed genomic PCR on *RPS19*, amplifying a region from the 5′UTR to intron 3 (Figure

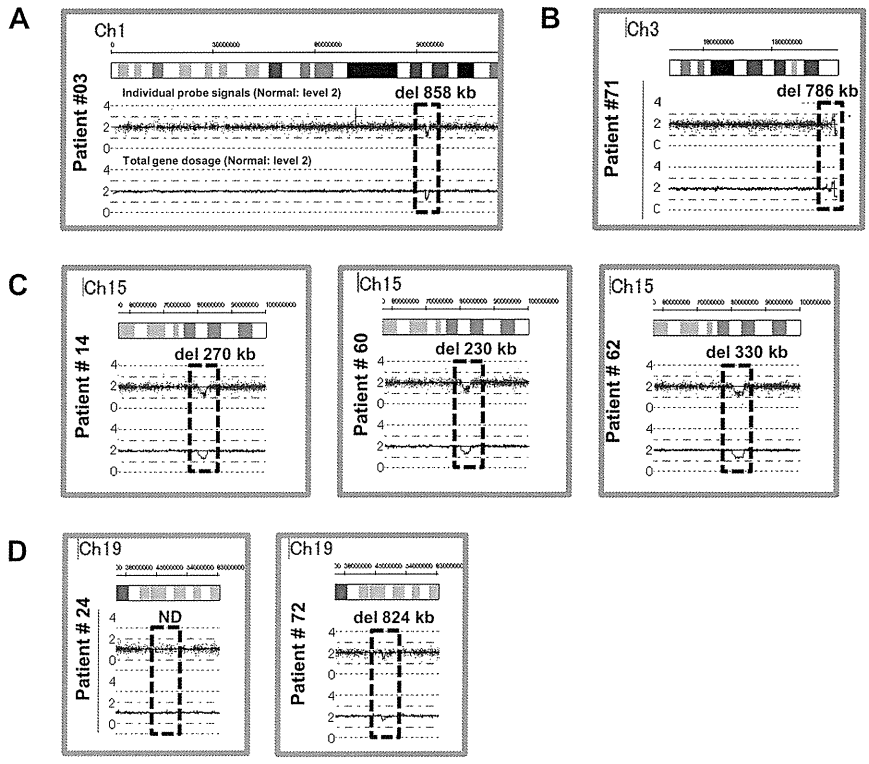

Figure 3. Results of SNP genomic microarray (SNP-chip) analysis. Genomic DNA of 27 Japanese DBA patients with unknown mutations was examined using a SNP array. Six patients had large deletions in their chromosome (ch), which included one DBA-responsible gene. Patient 3 has a large deletion in ch1 (A), patient 71 has a deletion in ch3 (B), patients 14, 60, and 62 have deletions in ch15 (C), and patient 72 has a deletion in ch19 (D).

4B). In patient 24, we observed an abnormally sized PCR product at a low molecular weight by agarose gel electrophoresis (Figure 4D). We did not detect a wild-type PCR product from the genomic PCR. This finding is probably because PCR tends to amplify smaller molecules more easily. However, we did detect a PCR fragment at the correct size using primers located in the supposedly deleted region. These bands were thought to be from the products of a wild-type allele. Sequencing of the mutant band revealed that intragenic recombination occurred at a homologous region of 27 nucleotides, from −1400 to −1374 in the 5′ region, to +5758 and +5784 in intron 3, which resulted in the loss of 7157 base pairs in the *RPS19* gene (Figure 4E). The deleted region contains exons 1, 2, and 3, and therefore the correct *RPS19* mRNA could not be transcribed.

Genotype-phenotype analysis and DBA mutations in Japan

Patients with a large deletion in DBA genes had common phenotypes (Table 4). Malformation with growth retardation (GR), including short stature or SGA, were observed in all 7 patients. In patients who had a mutation found by sequencing, half had GR (11 of 22; status data of DBA patients with mutations found by sequencing are not shown). GR may be a distinct phenotypic feature of large deletion mutations in Japanese DBA patients. Familial mutations were analyzed for parents for 5 DBA patients with a large deletion (patients 3, 24, 60, 62, and 72) by s-q-PCR. There are no large deletions in all 5 pairs of parents in DBA-responsible genes. Four of the 7 patients responded to steroid therapy. We have not observed significant phenotypic differences between patients with extensive deletions and other patients with regard to blood counts, responsiveness to treatment, or other malformations.

Discussion

Many studies have reported RP genes to be responsible for DBA. However, mutations have not been determined for approximately half of DBA patients analyzed. There are 2 possible reasons for this finding. One possibility is that patients have other genes responsible for DBA, and the other is that patients have a complicated set of mutations in RP genes that are difficult to detect. In the present study, we focused on the latter possibility because we have found fewer Japanese DBA patients with RP gene mutations (32.4%) compared with another cohort study of 117 DBA patients and 9 RP genes (approximately 52.9%).[4] With our newly developed method, we identified 7 new mutations with a large deletion in *RPL5*, *RPL35A*, *RPS17*, and *RPS19*.

The frequency of a large deletion was approximately 25.9% (7 of 27) in our group of patients who were not found to have mutations by genomic sequencing. Therefore, total RP gene mutations were confirmed in 42.6% of these Japanese patients (Table 5). Interestingly, mutations in *RPS17* have been observed at a high rate (5.9%) in Japan relative to that in other countries (1%).[5,15,16] Although the percentage of DBA mutations differs among different ethnic groups,[8,17-19] a certain portion of large deletions in DBA-responsible genes are likely to be determined in other countries by new strategies.

In the present study, we analyzed patient data to determine genotype-phenotype relations. To date, large deletions have been reported with RPS19 and RPL35A in DBA patients.[3,6,13] *RPS19* large deletions/translocations have been reported in 12 patients, and *RPL35A* large deletions have been reported in 2 patients.[19] GR in patients with a large deletion has been observed previously with *RPS19* translocations,[3,19-21] but it was not found in 2 patients with *RPL35A* deletion.[6] Interestingly, all of our patients with a large deletion had a phenotype

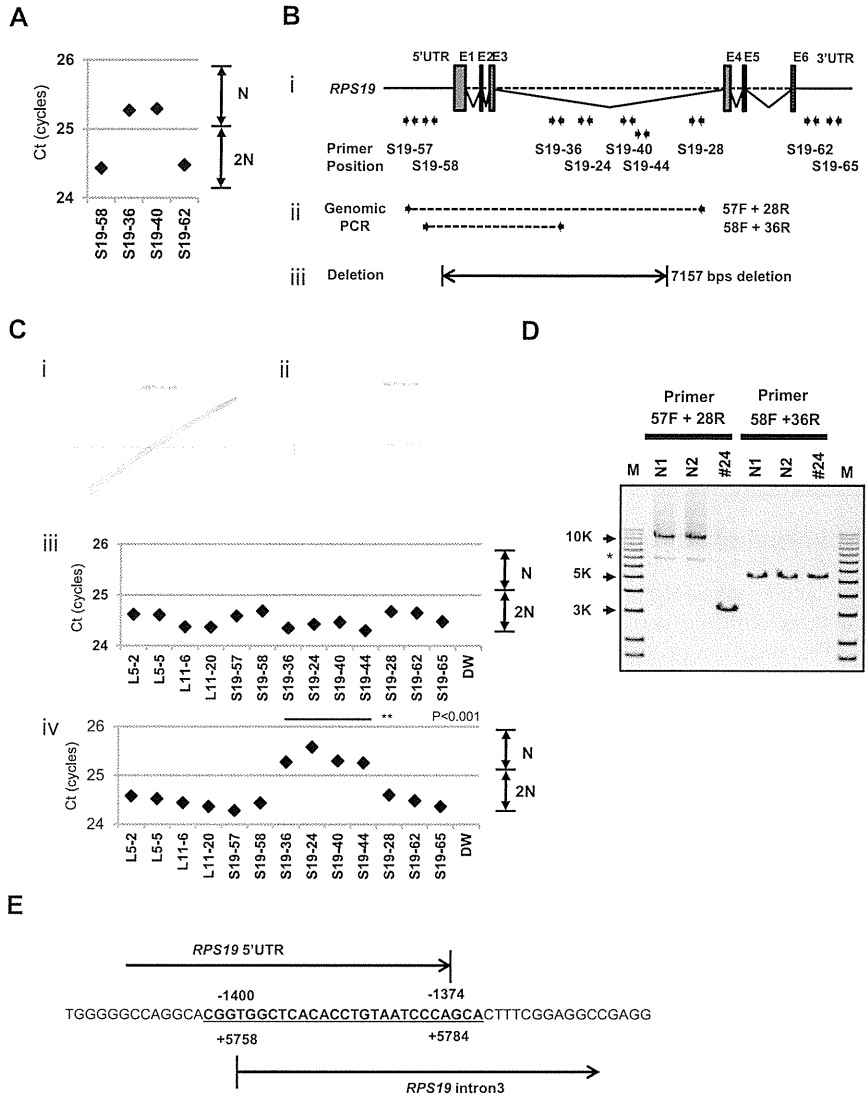

Figure 4. Result of s-q-PCR gene copy number assay for patient 24. (A) Results of s-q-PCR gene copy number assay for *RPS19* with 4 primer sets. (Bi) The *RPS19* gene copy number was analyzed with 9 specific primer sets for *RPS19* that span from the 5′UTR to the 3′UTR. (ii) Primer positions of genomic PCR for *RPS19*. (iii) Region determined to be an intragenic deletion in *RPS19*. (C) Results of gene copy number assay for *RPS19* show a healthy person (i,iii) and a DBA patient (ii,iv), and Ct results are shown (iii-iv). Patient 24 showed a "1-cycle delay" with primers located in the intron 3 region, but other primer sets were normal. (D) Results of genomic PCR amplification visualized by agarose gel electrophoresis to determine the region of deletion. N1 and N2 are healthy samples. *Nonspecific band. (E) Results from the genomic sequence of the 3-kb DNA band from genomic PCR on patient 24 showing an intragenic recombination from −1400 to 5784 (7157 nt) in *RPS19*. $^{**}P < .001$.

of GR, including short stature and SGA, which suggests that this is a characteristic of DBA with a large gene deletion in Japan. Our study results suggest the possibility that GR is associated with extensive deletion in Japanese patients. Although further case studies will be needed to confirm this possibility, screening of DBA samples using our newly developed method will help to advance our understanding of the broader implications of the mutations and the correlation with the DBA genotype-phenotype.

Table 5. Total mutations in Japanese DBA patients, including large gene deletions

Gene	Mutation rate
RPS19	12(17.6%)
RPL5	7(10.3%)
RPL11	3 (4.4%)
RPS17	4 (5.9%)
RPS10	1 (1.5%)
RPS26	1 (1.5%)
RPL35A	1 (1.5%)
RPS24	0
RPS14	0
Mutations, n (%)	29(42.6%)
Total analyzed, N	68

Copy number variation analysis of DBA has been performed by linkage analysis, and the *RPS19* gene was first identified as a DBA-susceptibility gene. Comparative genomic hybridization array technology has also been used to detect DBA mutations in *RPL35A*, and multiplex ligation-dependent probe amplification has been used for *RPS19* gene deletion analysis.[3,6,13,22] However, these analyzing systems have problems in mutation screening. Linkage analysis is not a convenient tool to screen for multiple genetic mutations, such as those in DBA, because it requires a high level of proficiency. Although comparative genomic hybridization technology is a powerful tool with which to analyze copy number comprehensively, this method requires highly specialized equipment and analyzing software, which limits accessibility for researchers. Whereas quantitative PCR–based methods for copy number variation analysis are commercially available (TaqMan), they require a standard curve for each primer set, which limits the number of genes that can be loaded on a PCR plate. To address this issue, a new method of analysis is needed. By stringent selection of PCR primers, the s-q-PCR method enables analysis of many DBA genes in 1 PCR plate and the ability to immediately distinguish a large deletion using the s-q-PCR amplification curve. In our study, 6 of 7 large deletions in the RP gene detected by s-q-PCR were confirmed by SNP arrays (Figure 3). Interestingly, we detected

1 large intragenic deletion in *RPS19*, which was not detected by the SNP array. This agreement between detection results suggests that the s-q-PCR copy number assay could be useful for detecting large RP gene deletions.

In the present study, 7 DBA patients carried a large deletion in the RP genes. This type of mutation could be underrepresented by sequencing analysis, although in the future, genome sequencing might provide a universal platform for mutation and deletion detection. We propose that gene copy number analysis for known DBA genes, in addition to direct sequencing, should be performed to search for a novel responsible gene for DBA. Although at present, it may be difficult to observe copy numbers on all 80 ribosomal protein genes in one s-q-PCR assay, our method allows execution of gene copy number assays for several target genes in 1 plate. Because our method is quick, easy, and low cost, it could become a conventional tool for detecting DBA mutations.

Acknowledgments

The authors thank Momoka Tsuruhara, Kumiko Araki, and Keiko Furuhata for their expert assistance.

This work was partially supported by grants-in-aid for scientific research from the Ministry of Education, Culture, Sports, Science and Technology of Japan, and by Health and Labor Sciences research grants (Research on Intractable Diseases) from the Ministry of Health, Labor and Welfare of Japan.

Authorship

Contribution: M.K. designed and performed the research, analyzed the data, and wrote the manuscript; A.S-O. and S. Ogawa performed the SNP array analysis; T.M., M.T., and M.O designed the study; T.T, K. Terui, and R.W. analyzed the mutations and status data; H.K., S. Ohga, A.O., S.K., T.K., K.G., K.K., T.M., and N.M. analyzed the status data; A.M., H.M., K. Takizawa, T.M., and K.Y., performed the research and analyzed the data; E.I. and I.H. designed the study and analyzed the data; and all authors wrote the manuscript.

Conflict-of-interest disclosure: The authors declare no competing financial interests.

Correspondence: Isao Hamaguchi, MD, PhD, Department of Safety Research on Blood and Biological Products, National Institute of Infectious Diseases, 4-7-1, Gakuen, Musashimurayama, Tokyo 208-0011, Japan; e-mail: 130hama@nih.go.jp; or Etsuro Ito, MD, PhD, Department of Pediatrics, Hirosaki University Graduate School of Medicine, 5 Zaifucho, Hirosaki, Aomori 036-8562, Japan; e-mail: eturou@cc.hirosaki-u.ac.jp.

References

1. Hamaguchi I, Flygare J, Nishiura H, et al. Proliferation deficiency of multipotent hematopoietic progenitors in ribosomal protein S19 (RPS19)-deficient diamond-Blackfan anemia improves following RPS19 gene transfer. *Mol Ther.* 2003;7(5 pt 1):613-622.
2. Vlachos A, Ball S, Dahl N, et al. Diagnosing and treating Diamond Blackfan anaemia: results of an international clinical consensus conference. *Br J Haematol.* 2008;142(6):859-876.
3. Draptchinskaia N, Gustavsson P, Andersson B, et al. The gene encoding ribosomal protein S19 is mutated in Diamond-Blackfan anaemia. *Nat Genet.* 1999;21(2):169-175.
4. Doherty L, Sheen MR, Vlachos A, et al. Ribosomal protein genes RPS10 and RPS26 are commonly mutated in Diamond-Blackfan anemia. *Am J Hum Genet.* 2010;86(2):222-228.
5. Gazda HT, Sheen MR, Vlachos A, et al. Ribosomal protein L5 and L11 mutations are associated with cleft palate and abnormal thumbs in Diamond-Blackfan anemia patients. *Am J Hum Genet.* 2008;83(6):769-780.
6. Farrar JE, Nater M, Caywood E, et al. Abnormalities of the large ribosomal subunit protein, Rpl35a, in Diamond-Blackfan anemia. *Blood.* 2008;112(5):1582-1592.
7. Gazda HT, Grabowska A, Merida-Long LB, et al. Ribosomal protein S24 gene is mutated in Diamond-Blackfan anemia. *Am J Hum Genet.* 2006; 79(6):1110-1118.
8. Konno Y, Toki T, Tandai S, et al. Mutations in the ribosomal protein genes in Japanese patients with Diamond-Blackfan anemia. *Haematologica.* 2010;95(8):1293-1299.
9. Robledo S, Idol RA, Crimmins DL, Ladenson JH, Mason PJ, Bessler M. The role of human ribosomal proteins in the maturation of rRNA and ribosome production. *RNA.* 2008;14(9):1918-1929.
10. Léger-Silvestre I, Caffrey JM, Dawaliby R, et al. Specific Role for Yeast Homologs of the Diamond Blackfan Anemia-associated Rps19 Protein in Ribosome Synthesis. *J Biol Chem.* 2005;280(46): 38177-38185.
11. Choesmel V, Fribourg S, Aguissa-Toure AH, et al. Mutation of ribosomal protein RPS24 in Diamond-Blackfan anemia results in a ribosome biogenesis disorder. *Hum Mol Genet.* 2008;17(9):1253-1263.
12. Flygare J, Aspesi A, Bailey JC, et al. Human RPS19, the gene mutated in Diamond-Blackfan anemia, encodes a ribosomal protein required for the maturation of 40S ribosomal subunits. *Blood.* 2007;109(3):980-986.
13. Quarello P, Garelli E, Brusco A, et al. Multiplex ligation-dependent probe amplification enhances molecular diagnosis of Diamond-Blackfan anemia due to RPS19 deficiency. *Haematologica.* 2008; 93(11):1748-1750.
14. Yamamoto G, Nannya Y, Kato M, et al. Highly sensitive method for genomewide detection of allelic composition in nonpaired, primary tumor specimens by use of affymetrix single-nucleotide-polymorphism genotyping microarrays. *Am J Hum Genet.* 2007;81(1):114-126.
15. Song MJ, Yoo EH, Lee KO, et al. A novel initiation codon mutation in the ribosomal protein S17 gene (RPS17) in a patient with Diamond-Blackfan anemia. *Pediatr Blood Cancer.* 2010;54(4):629-631.
16. Cmejla R, Cmejlova J, Handrkova H, Petrak J, Pospisilova D. Ribosomal protein S17 gene (RPS17) is mutated in Diamond-Blackfan anemia. *Hum Mutat.* 2007;28(12):1178-1182.
17. Cmejla R, Cmejlova J, Handrkova H, et al. Identification of mutations in the ribosomal protein L5 (RPL5) and ribosomal protein L11 (RPL11) genes in Czech patients with Diamond-Blackfan anemia. *Hum Mutat.* 2009;30(3):321-327.
18. Quarello P, Garelli E, Carando A, et al. Diamond-Blackfan anemia: genotype-phenotype correlations in Italian patients with RPL5 and RPL11 mutations. *Haematologica.* 2010;95(2):206-213.
19. Boria I, Garelli E, Gazda HT, et al. The ribosomal basis of Diamond-Blackfan Anemia: mutation and database update. *Hum Mutat.* 2010;31(12):1269-1279.
20. Campagnoli MF, Garelli E, Quarello P, et al. Molecular basis of Diamond-Blackfan anemia: new findings from the Italian registry and a review of the literature. *Haematologica.* 2004;89(4):480-489.
21. Willig TN, Draptchinskaia N, Dianzani I, et al. Mutations in ribosomal protein S19 gene and diamond blackfan anemia: wide variations in phenotypic expression. *Blood.* 1999;94(12):4294-4306.
22. Gustavsson P, Garelli E, Draptchinskaia N, et al. Identification of microdeletions spanning the Diamond-Blackfan anemia locus on 19q13 and evidence for genetic heterogeneity. *Am J Hum Genet.* 1998;63(5):1388-1395.

Frequent somatic mosaicism of *NEMO* in T cells of patients with X-linked anhidrotic ectodermal dysplasia with immunodeficiency

Tomoki Kawai,[1] Ryuta Nishikomori,[1] Kazushi Izawa,[1] Yuuki Murata,[1] Naoko Tanaka,[1] Hidemasa Sakai,[1] Megumu Saito,[2] Takahiro Yasumi,[1] Yuki Takaoka,[1] Tatsutoshi Nakahata,[2] Tomoyuki Mizukami,[3] Hiroyuki Nunoi,[3] Yuki Kiyohara,[4] Atsushi Yoden,[5] Takuji Murata,[5] Shinya Sasaki,[6] Etsuro Ito,[6] Hiroshi Akutagawa,[7] Toshinao Kawai,[8] Chihaya Imai,[9] Satoshi Okada,[10] Masao Kobayashi,[10] and Toshio Heike[1]

[1]Department of Pediatrics, Kyoto University Graduate School of Medicine, Kyoto, Japan; [2]Clinical Application Department, Center for iPS Cell Research and Application, Institute for Integrated Cell-Material Sciences, Kyoto University, Kyoto, Japan; [3]Division of Pediatrics, Department of Reproductive and Developmental Medicine, Faculty of Medicine, University of Miyazaki, Miyazaki, Japan; [4]Department of Pediatrics, Faculty of Medicine, Osaka University, Suita, Japan; [5]Department of Pediatrics, Osaka Medical College, Takatsuki, Japan; [6]Department of Pediatrics, Hirosaki University Graduate School of Medicine, Hirosaki, Japan; [7]Department of Pediatrics, Kishiwada City Hospital, Kishiwada, Japan; [8]Department of Human Genetics, National Center for Child Health and Development, Tokyo, Japan; [9]Department of Pediatrics, Niigata University, Niigata, Japan; and [10]Department of Pediatrics, Hiroshima University Graduate School of Biomedical Sciences, Hiroshima, Japan

Somatic mosaicism has been described in several primary immunodeficiency diseases and causes modified phenotypes in affected patients. X-linked anhidrotic ectodermal dysplasia with immunodeficiency (XL-EDA-ID) is caused by hypomorphic mutations in the *NF-κB essential modulator (NEMO)* gene and manifests clinically in various ways. We have previously reported a case of XL-EDA-ID with somatic mosaicism caused by a duplication mutation of the *NEMO* gene, but the frequency of somatic mosaicism of *NEMO* and its clinical impact on XL-EDA-ID is not fully understood. In this study, somatic mosaicism of *NEMO* was evaluated in XL-EDA-ID patients in Japan. Cells expressing wild-type NEMO, most of which were derived from the T-cell lineage, were detected in 9 of 10 XL-EDA-ID patients. These data indicate that the frequency of somatic mosaicism of *NEMO* is high in XL-ED-ID patients and that the presence of somatic mosaicism of *NEMO* could have an impact on the diagnosis and treatment of XL-ED-ID patients. (*Blood*. 2012;119(23):5458-5466)

Introduction

X-linked anhidrotic ectodermal dysplasia with immunodeficiency (XL-EDA-ID) is a disease with clinical features including hypohidrosis, delayed eruption of teeth, coarse hair, and immunodeficiency associated with frequent bacterial infections.[1-5] The gene responsible for XL-EDA-ID has been identified as *NF-κB essential modulator (NEMO)*.[6-8] NEMO is necessary for the function of IκB kinase, which phosphorylates and degrades IκB to activate NF-κB.[9-10] Defects in NEMO cause various abnormalities in signal transduction pathways involving NF-κB, and affect factors such as the IL-1 family protein receptors, the TLRs, VEGFR-3, receptor activator of nuclear factor κB (RANK), the ectodysplasin-A receptor, CD40, and the TNF receptor I.[7] Whereas a complete loss of NEMO function in humans is believed to cause embryonic lethality,[11] *NEMO* mutations in XL-EDA-ID patients are hypomorphic,[8] causing a partial loss of NEMO functions.

In XL-EDA-ID, NEMO defects lead to diverse immunologic features including susceptibility to pathogens, impaired Ab response to polysaccharides,[2,4,12] hypogammaglobulinemia,[13] hyper IgM syndrome,[14] and impaired NK-cell activity,[15] with a large degree of variability in phenotypes among the patients. For example, approximately one-tenth of XL-EDA-ID patients exhibit reduced mitogen-induced proliferation of T lymphocytes.[12] Moreover, one-fourth suffer from inflammatory disorders such as inflammatory bowel disease and rheumatoid arthritis,[12] although the inflammatory process usually relies on NF-κB activation.[16] One explanation for this clinical variability is that the XL-EDA-ID phenotype is *NEMO* genotype-specific. Although the XL-EDA-ID database reported by Hanson et al succeeds to some extent in linking the specific clinical features to *NEMO* genotype,[12] the penetrance of some clinical features is not high and the mechanism accounting for this variability is unknown.

Recently, we have reported a case of spontaneous reversion mosaicism of the *NEMO* gene in XL-EDA-ID, which showed an atypical phenotype involving decreased mitogen-induced T-cell proliferation along with decreased CD4 T cells (patient 1).[17] There have been no subsequent reports on somatic mosaicism in XL-EDA-ID, and its prevalence and impact on the clinical features of the disease is unknown. In this study, we describe the younger brother of patient 1, who suffered from XL-EDA-ID with the same mutation and somatic reversion mosaicism of *NEMO*. Patient 2 showed intriguing laboratory findings in that mitogen-induced T-cell proliferation varied in accordance with the rate of detected reversion in the peripheral blood. These 2 cases led us to perform a nationwide study of XL-EDA-ID patients in Japan that revealed a high incidence of somatic mosaicism of *NEMO*.

Submitted May 11, 2011; accepted April 8, 2012. Prepublished online as *Blood* First Edition paper, April 19, 2012; DOI 10.1182/blood-2011-05-354167.

The online version of this article contains a data supplement.

The publication costs of this article were defrayed in part by page charge payment. Therefore, and solely to indicate this fact, this article is hereby marked "advertisement" in accordance with 18 USC section 1734.

Table 1. Clinical and genetic features of XL-EDA-ID patients

Patient	Mutation	Ectodermal dysplasia	Mitogen-induced proliferation	Infections	Complications	Therapy	Sex chromosome chimerism
1	Duplication	+	Reduced	Sepsis (S.P. and P.A.)	Chronic diarrhea	IVIG	100% XY
				Disseminated M.A.C.	Failure to thrive	RFP, CAM, AMK, EB	
				Skin abscess (S.A.)	Small intestinal stenosis	Rifabutin	
				Invasive *Aspergillus*	Lymphedema		
2	Duplication	+	Reduced	Sepsis (*E coli*)	Failure to thrive	IVIG, ST, EB, CAM	99.8% XY 0.2% X
				Disseminated M.S.		Rifabutin, SCT	
3	D311E	−	Normal	Disseminated B.C.G.		IVIG, INH	100% XY
				Sepsis (S.P.)		RFP, SCT	
4	A169P	+	Normal	Meningitis (S.P.)	IBD	IVIG, ST, PSL	99% XY
					Interstitial pneumonia	CyA, MTX, Infliximab	
					Rheumatoid arthritis		
5	L227P	+	Normal	Recurrent pneumonia	IBD	ST, mesalazine	Not done
				Pyogenic coxitis		Infliximab	
				Recurrent otitis media			
6	R182P	+	Not done	Recurrent otitis media	IBD	ST, mesalazine	99.8% XY 0.2% X
				UTI, Recurrent stomatitis			
				Subepidermal abscess			
7	R175P	+	Normal	Recurrent sepsis (S.P.)		IVIG	100% XY
8	Q348X	+	Normal	Disseminated B.C.G.	IBD	IVIG, ST	100% XY
9	R175P	+	Normal	Recurrent pneumonia	IBD	IVIG	100% XY
				Recurrent otitis media		5-aminosalicylic acid	
				Kaposi varicelliform eruption			
10	1167 ins C	+	Normal	Sepsis and Enteritis (E.A)	Failure to thrive	IVIG, SCT	Not done
				Sepsis (C.G.)	Pyloric stenosis, colon polyps		
				UTI (K.P.)			

S.P. indicates *Streptococcus pneumoniae*; P.A., *Pseudomonas aeruginosa*; IVIG, intravascular immunoglobulin infusion; M.A.C., *Mycobacterium avium* complex; S.A., *Staphylococcus aureus*; *E coli*, *Escherichia coli*; ST, trimethoprim-sulfamethoxazole; M.S., *Mycobacterium szulgai*; AMK, amikacin; EB, ethambutol; CAM, clarithromycin; SCT, stem cell transplantation; B.C.G., Bacille de Calmette et Guerin; INH, isoniazid; RFP, rifampicin; IBD, inflammatory bowel disease; PSL, prednisolone; CyA, cyclosporine A; MTX, methotrexate; UTI, urinary tract infection; E.A., *Enterobacter aerogenes*; C.G., *Candida glabrata*; and K.P., *Klebsiella* pneumonia.

Methods

Informed consent

Informed consent was obtained from the patients and their families following the Declaration of Helsinki according to the protocol of the Internal Review Board of Kyoto University, which approved this study.

Patients

Patient 1 was an XL-EDA-ID patient with a duplication mutation of the *NEMO* gene spanning intron 3 to exon 6. This patient has been reported previously[17] and died from an *Aspergillus* infection at the age of 4. Patient 2, born at term, was the younger brother of patient 1. This patient was also diagnosed as XL-EDA-ID with the same duplication mutation as patient 1 by genetic study. He received trimethoprim-sulfamethoxazole prophylaxis and a monthly infusion of immunoglobulin from the age of 1 month. The patient maintained good health and had a body weight of 7899*g* at 6 months when he started to fail to thrive. Except for poor weight gain, patient 2 appeared active with a good appetite, negative C-reactive protein, normal white blood cell counts, and no apparent symptoms. At 19 months of age, *Mycobacterium szulgai* was detected by venous blood culture, and the patient was treated with multidrug regimens including ethambutol, rifabutin, and clarithromycin based on the treatment of systemic *Mycobacterium avium* complex infection. The patient responded well to the treatment and his weight increased from 7830*g* to 9165*g* within a month after the treatment was initiated. Patient 2 received an unrelated cord blood cell transplantation at 26 months of age, containing 8.5×10^7 nucleated cells/kg (4.4×10^5 $CD34^+$ cells/kg), which was matched at 5 of 8 loci: mismatches occurred at 1 HLA-B and 1 HLA-C allele (according to serology), and at 1 HLA-A, 1 HLA-B, and 1 HLA-C allele (according to DNA typing). The preconditioning regimen consisted of fludarabine (30 mg/m^2/d) on days −7 to −3, melphalan (70 mg/m^2/d) on days −6 to −5, and rabbit anti-thymocyte globulin (2.5 mg/kg/d) on days −6 to −2. At first, Tacrolimus (0.024 mg/kg/d) was used to prevent GVHD, but this was switched to cyclosporin A (3 mg/kg/d) on day 9 because of drug-induced encephalopathy. Neutrophil ($> 0.5 \times 10^9$/L) and platelet ($> 50 \times 10^9$/L) engraftment were examined on days 13 and 40, respectively. Although $CD19^+$ cells (2042/μL, 94% donor chimerism), $CD56^+$ cells (242/μL, 97% donor chimerism), and monocytes (557/μL, 69% donor chimerism) were successfully generated, $CD3^+$ cells were not detected in the peripheral blood by day 54. The patient suffered from septic shock and died on day 60. Patients 3 to 10 were XL-EDA-ID patients recruited nationwide in Japan. Clinical details of patients 3, 4, and 10 have been reported previously.[18-20] These patients had clinical phenotypes characteristic of XL-EDA-ID such as ectodermal dysplasia, innate and/or acquired immunity defects, and susceptibility to pyogenic bacteria and *Mycobacterium* infection. Every patient had a mutation in the *NEMO* gene that caused reduced NF-κB activation in a NEMO reconstitution assay, as described in "Proliferation of $NEMO^{normal}$ and $NEMO^{low}$ T cells." Patient profiles are listed in Table 1.

Flow cytometric analysis

NEMO intracellular staining was performed as previously described.[17] The cells were stained for the following lineage markers before staining for NEMO: CD4, CD8, CD14, CD15, CD19, CD56, CD45RA (BD Biosciences/BD Pharmingen), and CCR7 (R&D Systems Inc). Intracellular staining of human IFN-γ, TNF-α, and NEMO was performed as previously described.[18] The stained cells were collected using a FACSCalibur flow cytometer (BD Biosciences) and analyzed using the FlowJo software (TreeStar).

Reporter assay

Wild-type and mutant *NEMO* cDNAs were generated from a healthy volunteer and the recruited XL-EDA-ID patients by RT-PCR; the cDNAs were subcloned into the p3xFLAG-CMV14 vector (Sigma-Aldrich). NEMO null rat fibroblast cells (kindly provided by Dr S. Yamaoka, Department of Molecular Virology, Graduate School of Medicine, Tokyo Medical and Dental University, Tokyo, Japan) were plated at a density of